Belowground allocation and dynamics of recently fixed plant carbon in a California annual grassland soil

Christina Fossum[1*], Katerina Estera-Molina[1], Mengting Yuan[1], Don Herman[1], Ilexis Chu-Jacoby[1], Peter Nico[2], Keith Morrison[3], Jennifer Pett-Ridge[3,4], Mary Firestone[1,2]

Author Affiliations

[1]Department of Environmental Science, Policy, and Management, University of California, Berkeley, CA; [2] Earth Sciences Division, Lawrence Berkeley National Laboratory, Berkeley CA; [3]Physical and Life Sciences Directorate, Lawrence Livermore National Laboratory, Livermore, CA; [4]Life and Environmental Sciences Department, University of California, Merced, CA

Keywords: soil organic matter, annual grassland, $^{13}CO_2$ pulse labeling, SOM density fractionation, ^{13}C-NMR

Corresponding author: Mary Firestone, Department of Environmental Science, Policy, and Management, 140 Mulford Hall, University of California, Berkeley CA 94720 (mkfstone@berkeley.edu)

Summary

Plant roots and the organisms that surround them are a primary source for stabilized organic C, particularly in grassland soils, which have a large capacity to store organic carbon belowground. To quantify the flow and fate of plant fixed carbon (C) in a Northern California annual grassland, we tracked plant carbon from a five-day $^{13}CO_2$ pulse field labeling for the following two years. Soil and plant samples were collected immediately after the pulse labeling, and again at three days, four weeks, six months, one year, and two years. Soil organic matter was

fractionated using a sodium polytungstate density gradient to separate the free-light fraction (FLF), occluded-light fraction (OLF), and heavy fraction (HF). Using isotope ratio mass spectrometry, we measured ^{13}C enrichment and total C content for plant shoots, roots, soil, soil dissolved organic carbon (DOC), and the FLF, OLF, and HF. The HF was further analyzed by solid state ^{13}C NMR spectroscopy.

At the end of the labeling period, the largest amount of ^{13}C was recovered in plant shoots (60%), but a substantial amount (40%) was already found belowground in roots, soil, and soil DOC. Density fractionation of 4-week soil samples (from which living roots were removed) indicated that the highest isotope enrichment was in the mineral-rich heavy fraction, with similar enrichment of the FLF and OLF. At the 6-month sampling, after the dry summer period during which plants senesced and died, the amount of label in the FLF increased such that it was equal to that in the HF. By the 1-year sampling, ^{13}C in the FLF had declined substantially and continued to decline by the 2-year sampling. ^{13}C recovery in the OLF and HF, however, was qualitatively stable between sampling times. By the end of the 2-year experiment, 69% of remaining label was in the HF, 18% in the FLF and 13% in the OLF.

While the total ^{13}C content of the HF did not change significantly from the 4-week to the 2-year sample time, ^{13}C NMR spectroscopic analysis of spring HF samples from 2018, 2019, and 2020 suggests that the relative proportion of aliphatic/alkyl functional groups declined in the newly formed SOC over the 2-year period. Simultaneously, aromatic and carbonyl functional groups increased, and the proportion of carbohydrate groups remained relatively constant. In summary, our results indicate that initial associations between minerals and root-derived organic matter are significant and form rapidly; by 4 weeks, a substantial amount (17%) of the total plant-derived ^{13}C had become associated with the heavy fraction (HF) of soil. While the majority

of annual C input cycles rapidly (<2-year timescale), a sizeable proportion (~12% of the original inputs) persisted for 2 years.

1. Introduction

California annual grasslands occupy over 10 million ha (Heady et al., 1992), and have been predicted to be a more resilient and therefore effective carbon sink than California's fire-prone forests (Dass et al., 2018). According to a recent metaanalysis, grassland soils also have an increased capacity to store soil carbon in the face of increasing atmospheric CO_2 concentrations (Terrer-Moreno et al., 2020). As such, these ecosystems have become an attractive target for California state policy initiatives aimed at mitigating atmospheric CO_2 levels through soil carbon sequestration (Biggs & Huntsinger, 2021; Baker et al., 2020). However, our scientific understanding of soil carbon cycling, the fate of plant residues belowground, and how annual grasslands can broadly act as a viable carbon sink remains incomplete (Bradford et al., 2019). To effectively manage carbon stocks, further research is required to better understand the ecological parameters that regulate soil carbon cycling in these globally significant ecosystems.

Belowground carbon dynamics in California annual grasslands reflect the annual plant life cycle (Eviner & Firestone, 2007). Plant communities are dominated by annual grasses and forbs, species whose reproductive strategies are well-adapted to a Mediterranean climate where seasonal moisture limitations largely regulate nutrient cycling. This climate is characterized by cool wet winters and a warm summer period with no rainfall, a defining feature of which is the misalignment of two critical conditions for plant growth: rainfall and solar energy. Moisture

limits plant growth in the summers, and sunlight and temperature limit plant growth in the winters (Bartolome et al., 2007; Eviner and Firestone, 2007). The plant life cycle begins with the first germinating rainfall in the autumn, proceeds slowly through the winter due to sunlight and temperature limitations, peaks in the spring when both soil moisture and sunlight are usually optimized, and ends with plant senescence once soil moisture has declined with the onset of the summer dry period (Eviner 2016; Eviner and Firestone, 2007). Throughout the winter/spring growing season, carbon enters the soil primarily via a constant "drip" of plant root exudation (Sokol & Bradford, 2019; Pett-Ridge et al., 2021); over the summer dry period, plant senescence and subsequent litter input, coupled with low-moisture conditions drives the transient accumulation of litter; in the autumn at the onset of the rainy season, a large portion of accumulated carbon is rapidly released as CO_2 in a decomposition "pulse" (Blankinship & Schimel, 2018).

The characteristic seasonal soil moisture variability in Mediterranean climates can impact the persistence of soil organic matter (SOM) via multiple mechanisms. Following 4-6 months of no precipitation, autumn's first major rainfall event strongly impacts the soil biota, physically stresses soil aggregates, chemically alters soil minerals, and destabilizes SOM, driving a pulse of respiration known as the Birch Effect (Barnard et al., 2020; Blazewicz et al., 2020; Birch, 1958). This release of CO_2 is generally understood to result from the stimulation of microbial respiration and high availability of substrate (Schimel, 2018; Barnard et al., 2020). Plant germination usually occurs in the Autumn, temperature limits growth in the winter, and the peak period of plant growth occurs in the spring when both temperature and moisture are optimized. The majority of rhizosphere-derived SOC generation occurs during this spring growth period. Then, in late spring when soil moisture conditions no longer support growth, new root C inputs

decline as plant senescence occurs and annual species set seed. During this dry-down period, decreasing soil moisture reduces hydrological connectivity between soil pores, isolating microbes from carbon substrates and resulting in a decline in ecosystem activity (Manzoni and Katul, 2014; Barnard et al., 2013; Blankinship and Schimel, 2018). Decomposition of plant biomass and transfer of carbon belowground continue to be limited throughout the summer dry period (Chou et al., 2008; Eviner and Firestone, 2007). While not fully understood, these wet-dry cycles characteristic of California annual grasslands may be important drivers of SOM persistence, and may be susceptible to future climate conditions that either amplify or minimize their stabilizing or destabilizing effects (Bailey et al., 2019).

Soil carbon is often considered in terms of distinct soil organic matter "pools": either associated with minerals, occluded within microaggregates, or "free" (not subject to either chemical or physical protection) (Poeplau et al., 2018). Recent studies have shown that labile carbon substrates can play an important role in SOM formation and stabilization in both physically (occluded) and chemically (mineral-associated) pools (Cotrufo et al., 2015; Totsche et al., 2017; Villarino et al., 2021), while plant litter is generally understood to largely comprise the free-light fraction material. The mineral-associated or "heavy fraction" is of particular interest for soil organic carbon persistence; it is typically the oldest distinct pool (Torn et al., 1997) and represents carbon stabilized via mineral sorption and co-precipitation mechanisms (Kogel-Knabner et al., 2008). This fraction of SOM, commonly termed MAOM (mineral-associated organic matter) (Cotrufo et al., 2019), is largely of microbial origin and thought to be derived from relatively labile C substrates (Clemente et al., 2011; Cotrufo et al., 2013; Villarino et al., 2021). Recent work has suggested that microbial necromass may be a primary precursor to stable organic matter in grasslands (Angst et al., 2021).

In this study, we followed plant-fixed C entering the soil and moving into various soil organic matter pools, and also tracked its form and transformations over the course of multiple growing seasons. Initially, we exposed soil to the stable isotope ^{13}C, via a 5-day $^{13}CO_2$ field labeling of a California annual grassland plant community. To quantify the distribution and two-year dynamics of added ^{13}C tracer in aboveground plant biomass, plant roots, soil, and various soil organic matter pools, we sampled biomass and soil at multiple timepoints following the field pulse labeling (immediately, 3 days, 4 weeks, 6 months, 1 year, and 2 years), and physically fractionated soil samples with a sodium polytungstate density gradient procedure. We isolated 3 soil density fractions: (HF) the heavy fraction (mineral-associated soil organic matter, MAOM), (OLF) the occluded-light fraction (micro-aggregate occluded soil organic matter), and (FLF) the free-light fraction (accessible soil organic matter debris) (Golchin et al., 1994; Sollins et al., 2009). We further characterized the chemistry of the heavy fraction ^{13}C using solid state CPMAS ^{13}C NMR spectroscopy, in order to better understand both the composition of carbon newly incorporated into this fraction, as well as the influence of new inputs on the total mineral-associated carbon pool. By combining ^{13}C labeling, soil density fractionation, and solid-state ^{13}C NMR, we sought to temporally characterize the flow and fate of newly fixed C entering this annual grassland soil and understand the dynamics of plant-derived soil organic carbon formation and persistence.

2. Methods

2.1 Field site description

Field work was conducted at the University of California Hopland Research and Extension Center (HREC), in southwestern Mendocino County, CA (39.004056, -123.085872).

Climatic conditions at the field site are similar to conditions across Mediterranean California, with cool and wet winters, and hot, dry summers. Germination of the annual plant community occurs in the fall, following the first significant rainfall of the winter rainy season. Growth is limited throughout much of the winter by sunlight and temperature, and then peaks in the spring, followed by seed production and senescence by early summer (Becchetti et al., 2016). The vegetation community is dominated by naturalized annual grass and forb species including *Avena spp*., *Festuca spp.*, *Erodium spp.*, and *Bromus spp.* (Bartolome et al., 2007). Today, HREC is operated by the UC system as a working sheep ranch. Our field plots have been fenced off from grazing for >20 years. The soil at our field site belongs to the Squawrock-Witherell complex, a loamy-skeletal, mixed, superactive, thermic Typic Haploxeralf. Underlying parent material is colluvium derived from sandstone (Soil Survey Staff, 2020). Our measurements suggest the dominant clays are muscovite, chlorite, and kaolinite; dominant non-clay minerals are quartz and plagioclase (Table 1).

2.2 Experimental design

Samples collected for this study are a subset from a larger $^{13}CO_2$ labeling and precipitation manipulation field experiment. In the spring of 2017, sixteen 3.24 m^2 plots were established, each delineated by a 1-m deep plastic liner to limit soil water equilibration with surrounding soils, and each containing six 40-cm diameter circular subplots. Circular subplots were surrounded by a 15cm deep PVC "collar" designed to be fitted with an above-ground cylindrical chamber for labelling plants with either ^{12}C or ^{13}C-CO_2 (Supplemental Figure 1A). Each circular subplot was subdivided into four 15-cm deep sections via plexiglass dividers; this "wedge" design allowed us to destructively harvest $^{13}CO2$-labeled soil and biomass from a single circular subplot at multiple timepoints following a labeling event (Supplemental Figure 1B).

Removable rain-exclusion shelters were installed above all plots and precipitation manipulation began in the fall of 2017 and continued through the 2019-2020 growing season. Of the 16 plots, eight received 50% of average annual precipitation and eight received 100%, where average annual rainfall was calculated from precipitation data collected at HREC dating back to 1951 (Supplemental Figure 2). Depending on the timing and quantity of natural rainfall events, field plot precipitation was augmented via manual watering with natural spring water and limited through application of the rain-out shelters.

Experimental plots were labeled with ^{12}C or ^{13}C-CO_2 (99 atm %, Cambridge Isotopes) for 5 days from February 11-15, 2018, timed to correspond with the expected maximum root development phase of *Avena spp.* plant growth (the plots were seeded the prior year to encourage a *Avena spp.* dominated community). CO_2 levels during the pulse labeling event were monitored with a Picaroon G2200-I analyzer (for ^{13}C) and infrared gas analyzer (IRGA) (for ^{12}C). For the labeling, well-sealed cylindrical chambers made of PAR transmissive PVC film were fitted over two circular subplots per plot (Supplemental Figure 1A). Plants within these chambers were exposed to either $^{12}CO_2$ or an isotopically labeled analog, $^{13}CO_2$, resulting in 16 $^{12}CO_2$-labeled 'control' subplots and 16 $^{13}CO_2$-labeled subplots. The headspace CO_2 concentrations within the chambers were maintained between 400-1500ppm during the daytime, and chambers were removed from plots at night. ^{13}C enrichment of $^{13}CO_2$-labeled subplots was maintained between 30-75 atom%. Within each CO_2 group, 8 of the 16 subplots were under the 50% precipitation regimen, and 8 under the 100% regimen.

2.3 Field harvests of ^{13}C labeled biomass and soil

Soil was harvested at six times following the $^{13}CO_2$ labeling event: (1) immediately after the 5-day labeling period, (2) three days later, (3) four weeks after the first harvest, (4) six months after the first harvest, (5) one year after the first harvest, and (6) two years after the first harvest. We subsequently refer to these harvest sampling times both by the time elapsed since the ^{13}C labeling event (0 days, 3 days, 4 weeks, 6 months, 1 year, and 2 years), as well as by the season in which the harvest occurred: Spring '18 (4 weeks), Fall '18, Spring '19, and Spring '20. At each sampling time, we harvested 4 replicate samples from each experimental treatment: ^{12}C-labeled, ^{13}C-labeled, 50% precipitation, 100% precipitation. We did not detect a statistically significant ($p < 0.05$) precipitation treatment effect on any soil or plant characteristics measured in this study; thus, replicates from these treatments were pooled for final analyses such that n=8 for most of the analyses presented.

Root and shoot biomass samples were collected at three times following the $^{13}CO_2$ pulse labeling: (1) at zero days, when we expected the maximum ^{13}C-labeled shoot biomass, (2) at three days, and (3) at four weeks, by which point we expected a measurable fraction of ^{13}C label to have been translocated to root biomass and the surrounding soil. Shoot biomass was collected by clipping all live aboveground plant tissue from a single subplot "wedge", and then scaling up to g / m^2. Root biomass was collected from three 2.45-cm cores that were installed in each wedge at the time of harvest and scaling up to the full wedge volume (1/4 X 40cm subplot X 15cm depth), and then g / m^2. Prior to the 6-month sampling time (Fall18), aboveground litter remaining from the 2017-2018 growing season was removed from the plots.

At each of the first four sampling times, we harvested 16 "wedges" of soil. Once soil wedges were harvested, visible roots were removed and soil was homogenized, 500g sub-samples were collected, air-dried, and stored at ambient temperature for further analysis. At each

of the final two sampling times (Spring19 and Spring20), we harvested two cores per wedge (2.54 cm diameter X 15cm deep) rather than the whole wedge to preserve the remaining soil for future experiments, however, we harvested the same number of samples as in the previous two harvests. In these two cores we removed roots and homogenized the soil (~300g) as above, then air dried and stored the soil for further analyses. Additional subsamples at each of the four harvests were immediately aliquoted from homogenized soil for analyses requiring fresh soil.

Altogether, eight ^{13}C-labeled and eight ^{12}C-labeled shoot, root, and soil samples were harvested at 0 days, 3 days, and 4 weeks after labeling. Senescence of ^{13}C-labeled plants occurred over the summer of 2018, between the 4-week and 6-month sampling times. Therefore, for the remaining sampling times (6-month, 1-year, and 2-year), only soil samples were collected (eight ^{13}C-labeled and eight ^{12}C-labeled).

2.4 Processing and diagnostic analyses of soil, root, and shoot biomass

Aboveground biomass dry weight was determined by drying harvested biomass at 65 °C until a stable dried weight was achieved. Root biomass dry weight was determined by hand picking live roots from collected root biomass cores, washing, and drying at 65 °C until dried weights reached a stable plateau. Dry root biomass per wedge was then calculated by scaling the dried root weights to the volume of the wedge.

Soil pH was determined in a 1:1 ratio of fresh homogenized soil to 0.01M $CaCl_2$. Soil gravimetric water content was assessed by drying a 10g subsample of fresh homogenized soil at 105 °C until dried weights reached a stable plateau when weighed, then calculating percent water. DOC was extracted from 5g fresh soil with 20ml 0.5M K_2SO_4; DOC and ^{13}C-DOC was assessed by the Yale Analytical and Stable Isotope Center (YASIC) via wet oxidation method

(Lang et al., 2012). Remaining analyses were conducted on homogenized air-dry soil. Soil texture analysis was conducted by the UC Davis Analytical Lab via the hydrometer method (Sheldrick et al., 1993). Aggregate stability was conducted using a wet sieving method previously adapted by Sher et al. (2020), using a custom wet-sieve apparatus (Singer et al., 1992; Sher et al., 2020).

2.5 Soil quantitative X-ray diffraction analysis

Soil mineralogy was determined at Lawrence Livermore National Lab (Zhou et al., 2018). Soil samples were dried, crushed and passed through a 500 μm sieve. Then 3 grams of soil was ground with 15 mL of methanol in a McCrone mill with corundum grinding elements for 5 minutes. The sample was transferred into a plastic tray, air dried and homogenized on a vortex mixer with 10 mm plastic beads for 3 minutes (Bakker et al., 2018). The random powders were then side loaded into XRD sample holders and analyzed on a Bruker D8 advance XRD scanning from 3 to 65° 2Θ with a step size of 0.011° at a rate of 5 seconds per step. Quantitative analysis was done using BGMN Rietveld refinement and the Profex interface software (Doebelin et al., 2015). The XRD patterns were refined to fit crystal unit cell parameters, size, site occupancy and preferred orientation.

2.6 Soil density fractionation

Soil density fractionation was performed on samples collected at 4-weeks, 6-months, 1-year, and 2-year sampling times. Air-dried soil was sieved to 2mm before being density fractionated into three discrete pools of soil organic matter using a sodium polytungstate (SPT) density gradient: free-light fraction (FLF, $\rho < 1.75 g\text{-}cm^{-3}$), occluded-light fraction (OLF, $\rho < 1.75 g\text{-}cm^{-3}$), and mineral-associated or heavy fraction (HF, $\rho > 1.75 g\text{-}cm^{3}$). The density of

248 1.75g-cm^{-3} was chosen due to the similarities in mineralogy and soil physical characteristics
249 between this sampling site and the site sampled in *Neurath et al., 2021*, which used this same
250 SPT approach.

251 The method for density fractionation used in our study was adapted from Hicks Pries et
252 al. (2017), previously adapted from Strickland & Sollins (1987). For each sample, 50mL of
253 sodium polytungstate (SPT-0, Geoliquids) prepared to a density of 1.75g-cm^{-3} was added to a
254 250mL centrifuge tube containing 20g of air-dried soil. The mixture was inverted by hand to
255 ensure all soil came into contact with the SPT; soil remaining on the lid and sides was rinsed
256 down with an additional 50mL of SPT. The SPT-soil solutions were allowed to settle for 1 hour,
257 then centrifuged for 1 hour at 3,700 RCF in a swinging bucket rotor (Beckman Avant J-20 Floor
258 Centrifuge with JS-5.3 rotor). Following centrifugation, samples were allowed to settle again
259 until no particles remained suspended within the SPT solution. Particles floating on top of the
260 SPT solution were defined as the FLF and were isolated by aspirating onto a 0.7μm glass
261 microfiber filter (Wattman), and rinsed with MilliQ water to remove residual SPT. Then, the
262 FLF filters were transferred into drying tins in a 55 °C oven until standing water had evaporated.

263 To release the OLF from microaggregates, the remainder of the soil-SPT mixture was
264 mixed with a benchtop mixer for 1 minute, followed by sonication for 90 seconds. As above, the
265 soil was then rinsed, allowed to settle, centrifuged for 1 hour, and the floating fraction isolated
266 via aspiration and dried.

267 The remaining sediment (ρ > 1.75g-cm^{-3}) was defined as the HF. This fraction was rinsed
268 with 150mL Milli-Q H2O, vigorously shaken by hand, centrifuged for 20 minutes, followed by
269 aspiration and disposal of the supernatant. This was repeated 5 times, or until the density of the

supernatant ~ 1g-cm^{-3}. The HF was transferred into drying tins and dried at 55 °C. Once standing water had evaporated, all three fractions were transferred into a 105 °C oven for 48 hours. Oven-dried samples were cooled in a desiccator before being weighed, ground with a mortar and pestle, and stored in glass vials.

2.7 Isotopic and elemental analysis

Prior to elemental analysis, samples were ground to a fine powder and weighed into aluminum tins, with sample weight proportional to expected carbon content (4mf for the FLF, 2mg for the OLF, 50mg for the HF and bulk soil, 0.35mg for shoot biomass, and 0.30mg for root biomass samples). Bulk and density fractionated soil were ground using a mortar and pestle, aboveground biomass was ground using a coffee grinder, and root biomass was ground by hand. Total C, N, and ^{13}C enrichment were measured via total combustion using an elemental analyzer coupled with a continuous flow Isotope Ratio Mass Spectrometer (IRMS) at the Stable Isotope Facility at the University of California, Davis (AOAC Official Method 972.43).

2.8 ^{13}C-NMR

Subsamples of heavy fraction (HF) material were analyzed by ^{13}C-NMR to assess broad chemical composition of mineral-associated organic matter. Solid-state ^{13}C cross polarization magic angle spinning (CPMAS) spectroscopy was run on one ^{13}C-labeled HF sub-sample from the 4-week, 1-year, and 2-year sampling times, as well as one ^{12}C-labeled control HF subsample from the 4-week timepoint as a control comparison. These four spectra were acquired using a 4mm log-gamma CPMAS probe on a 500 MHz Bruker Avance 1 NMR spectrometer at the UC Davis NMR facility. Samples were spun at 10 kHz with an acquisition time of 41 ms. Scan number ranged from 75,000 – 102,400. Glycine (176ppm) was used as the external reference.

Using Topspin software, data were zero filled to 8k; an exponential function with 500 Hz of line broadening was used for signal processing, with zero order phase correction, followed by manual baseline correction.

Broad C functional groups were defined based on the following chemical shift regions: aliphatic/alkyl C (0-45ppm), O-alkyl C (45-110ppm), aromatic and aryl C (110-162ppm), and carbonyl C (162-190ppm) (Helfrich, 2006). Integration of chemical shift regions was conducted using Topspin 3 software to calculate relative contribution of different functional group regions to total peak area (0-190ppm).

2.9 Statistical analyses

Effect of sampling time on C, N, and ^{13}C content was determined using ANOVA. Statistical significance was determined using Tukey's HSD post-hoc test with the R package 'agricolae' (Mendiburu, 2015). Data was visualized using the R package 'ggplot2' (Wickham, 2016).

2.10 Calculation of ecosystem ^{13}C assimilation

We define ecosystem assimilated ^{13}C as that quantifiable in (1) aboveground (plant biomass) and (2) belowground (soil + root biomass) pools, in other words net ^{13}C gain rather than gross ecosystem exchange. Ecosystem ^{13}C assimilation was calculated by converting the ^{13}C concentration of each pool (aboveground biomass, root biomass, soil in mg / g) to quantity (g ^{13}C / m^2 over a 15cm sampling depth) and then summing. For simplicity, the sum of ^{13}C recovered in aboveground biomass plus soil and root biomass immediately after the pulse labeling period (0-days) was interpreted to equal 100% of assimilated ^{13}C. The percentage of assimilated ^{13}C remaining at each subsequent sampling timepoint was then calculated relative to this original

amount (Table 2). We note that, at the 6-month, 1-year and 2-year sampling times, ^{13}C-labeled aboveground biomass and roots had senesced and the aboveground pool was not measured, and roots were not physically separately from the soil as was done for the 0-days and 4-weeks timepoints. Average ^{13}C recovery based on summing the FLF + OLF + HF was approximately 72% that of the bulk soil, which is within the range for density fractionated soil C recovery values cited in the literature (Crow et al., 2007; Cusack et al., 2018).

3. Results

3.1 Ecosystem ^{13}C Incorporation

Immediately following the $^{13}CO_2$ labeling period, all four ecosystem pools that we analyzed (soil, shoot and root biomass, DOC) were enriched in ^{13}C (Figures 1, 2). We defined the total amount of ^{13}C present at the 0-day to be 100% and calculated pools thereafter relative to this starting point. During the 5-day labeling period, over 12g ^{13}C / m^2 derived from plant photosynthate had accumulated in these ecosystem pools, accounting for roughly 0.2% of total ecosystem C content (aboveground biomass, root biomass, and soil in the 0-15cm depth horizon). By 4 weeks, shoot biomass ^{13}C content had declined to 61.7% of the initial amount ($p = 0.015$) (Figure 1, Table 2). Transfer of plant-fixed ^{13}C to belowground pools was immediate, accounting for 40% of total ecosystem ^{13}C immediately after the labeling. Belowground ^{13}C content reached a peak 6 months post-labeling. Between the 6-month, 1-year, and 2-year sampling times, assimilated ^{13}C in the ecosystem decreased stepwise: 64% of the original ^{13}C remained at 6 months, 37% at 1 year, and 23% at 2 years (Figure 1, Table 2).

Samples collected at 0 days, 3 days, and 4 weeks following $^{13}CO_2$ labeling were used to assess the initial dynamics of ^{13}C in shoots, roots and DOC (Figure 2). Shoot ^{13}C enrichment (g

336 ^{13}C / m^2) declined significantly over the 4 weeks post labeling. While not statistically significant
337 at $p < 0.05$, mean shoot biomass ^{13}C appeared to decline slightly by 3 days post-labeling, despite
338 no detectable change in shoot biomass--possibly due to loss of recently fixed ^{13}C via plant
339 respiration. Allocation of ^{13}C-labeled photosynthate to the roots occurred immediately, and did
340 not significantly change over the 4 weeks, despite expected dilution of the atom-% ^{13}C by
341 continued root growth. ^{13}C enrichment of the DOC pool did not significantly change between 0
342 days, 3 days, and 4 weeks following the $^{13}CO_2$ labeling event.

343 **3.2 Soil Density Fractions**

344 We used density fractionation to assess changes in the quantity of newly-fixed plant-
345 derived C in soil samples collected in March of 2018 (Spring18 = 4-week sampling time), the
346 Fall of 2018 (Fall18 = 6-month), April of 2019 (Spring19 ~ 1-year), and March of 2020
347 (Spring20 ~ 2-year). Of the three fractions assessed, the HF accounted for roughly 99% of the
348 total recovered soil mass (Table 3) and contained the highest amount of C, accounting for 66%
349 of the total on average, while the OLF was 20%, and FLF 14% (Figure 3). The distribution of
350 total N followed a similar pattern to total C, but with an even greater proportion of N
351 accumulating in the HF (Table 3): 83% in the HF, 10% in the OLF, and 7% in the FLF. The C:N
352 ratio varied significantly by fraction type: highest in FLF (~20:1), intermediate in OLF (~18:1),
353 and lowest in HF (~8:1), and these differences were statistically significant ($p < 0.05$). Total C,
354 N, and C:N (Table 3, Figure 3) did not exhibit detectable seasonal fluctuations between the
355 Spring and Fall sampling times. For all density fractions, total C was generally lower at the
356 Spring20 sampling than at other sampling times (Figure 3).

357 The ^{13}C labeling event occurred during the growing season in February 2018, and
358 samplings occurred in Spring 2018, Fall 2018, Spring 2019, and Spring 2020. Four weeks after
359 the ^{13}C labeling, 24% of the initial ecosystem ^{13}C was recovered in soil density fractions (Table
360 2). Of that, significantly more was recovered in the HF than in the OLF or FLF. While
361 accumulation of total C was higher in the OLF than FLF, ^{13}C was in the FLF at the 4-week
362 sample time. ^{13}C enrichment (atom-% ^{13}C) was generally highest in the FLF and lowest in the
363 OLF. Between the 4-week and 6-month sampling times, soil organic ^{13}C-labeled carbon ($SO^{13}C$)
364 recovered in the density fractions roughly doubled, with the majority of additional $SO^{13}C$
365 accumulating in the FLF (Figure 3, Table 2). At 6 months, the amount of ^{13}C recovered in the
366 FLF was similar to that in the HF. Between 6 months and 1 year after labeling, $SO^{13}C$ content of
367 the density fractions declined by 40%, with a particularly large decrease observed in FLF
368 material. The 2-year ^{13}C recovery in the soil density fractions was 55% of that recovered in the
369 1-year samples. By Spring20, over two years after the original ^{13}C addition, isotopically labeled
370 carbon persisted in all three fractions, with over 50% of the remaining ecosystem ^{13}C
371 (representing 13.5% of the initial ecosystem ^{13}C content) found in protected forms, either
372 occluded within soil microaggregates (OLF) or associated with soil minerals (HF) (Table 2).

373 **3.3 ^{13}C NMR analysis of mineral-associated carbon**

374 Heavy fraction (HF) material from 4-week, 1-year, and 2-year sampling times was
375 analyzed by ^{13}C NMR to assess the molecular forms taken by the newly fixed ^{13}C and present in
376 the HF. Likely due to the presence of paramagnetic minerals in these soils, the peaks in the ^{13}C
377 NMR spectra were broad and hence we were not able to identify specific compounds. Instead,
378 we assessed relative proportions of broad chemical classes based on chemical shift regions in the

NMR spectra: alkyl C 0-45ppm, O-alkyl C 45-110ppm, aromatic C 110-162ppm, and carbonyl C 162-190ppm (Figure 4, Supplemental Figure 5).

Labeling plants with $^{13}CO_2$ allowed us to follow the functional group characteristics of newly fixed C incorporated into the mineral-associated pool (Figure 4). The SO^{13}C-HF appeared to be relatively enriched in alkyl C with lesser amounts of aromatic and carboxyl C. In the ^{13}C NMR spectra, the relative proportion of alkyl C declined over time from 4 weeks to 1 year to 2 years after the ^{13}C labeling period. Over this same period, the relative proportion of carboxyl C increased, while the relative proportion of aromatic C and O-alkyl C remained constant. While the proportion of C functional groups in the ^{13}C-labeled HF material was distinct from the ^{12}C-labeled control HF material at all sampling times, the relative proportions of C functional groups in the ^{13}C-labeled material appeared to become more similar to those observed in the control material over time.

4. Discussion

4.1 Ecosystem ^{13}C Incorporation

In this California annual grassland soil, growing plants quickly allocated a substantial proportion of photosynthate belowground. We traced the translocation of plant photosynthate to belowground carbon pools during a 5-day $^{13}CO_2$ field labeling (Figure 1). Our labeling period occurred in late winter (February 11-15, 2018), which was intended to correspond to the plant growth stage of maximum allocation of aboveground photosynthate C to root growth (Jackson et al., 1989). By the end of this 5-day period, 40% of assimilated ^{13}C had been allocated belowground (Figure 1).

400 ^{13}C recovery in plant roots is a clear indication of the incorporation of fresh plant-derived
401 carbon inputs into the soil, particularly as these ^{13}C-labeled roots decompose over time. We
402 observed evidence of this phenomenon at the 6-month sampling time, when ^{13}C recovery in FLF
403 material reached its peak. We presume this was primarily due to incorporation of ^{13}C labeled root
404 litter from the previous growing season. However, at the 4-week sampling time, we already
405 observed high ^{13}C recovery (nearly 38%) in all our soil density fractions, from which we had
406 removed live roots. This suggests that substantial ^{13}C was exuded into the soil by the roots
407 during this period of plant growth, or that other types of rhizodeposits (sloughed root tip cells,
408 cell hairs) had become part of the soil's organic matter pools (Table 2).

409 In our study, the ^{13}C enrichment of root tissue was similar to the enrichment of the DOC
410 pool when measured either immediately or 3 days after the end of the labeling period (Figure 2).
411 This suggests that root exudates were in equilibrium with root biomass enrichment during this
412 plant growth stage. By the 4-week sampling time, ^{13}C enrichment appears to slightly increase in
413 plant roots and decline in soil DOC (although neither increase nor decrease was statistically
414 significant), which could imply a shift of plant C allocation from labile root exudates, to root
415 structural compounds. Furthermore, we observed a slight decline in belowground ^{13}C content
416 between 0 days and 4 weeks following the ^{13}C labeling (Figure 1), which is likely from root and
417 microbial respiration. These findings indicate that as plants continue to grow, recently-fixed
418 photosynthate was rapidly translocated within the plant and released into the soil as labile C
419 compounds exuded by roots (and perhaps also by associated arbuscular mycorrhizal fungi
420 (AMF) (Kakouridis et al., 2021)). Almost just as rapidly, these labile exudates are metabolized
421 by the active rhizosphere microbial communities (Waldrop & Firestone, 2006).

We found that total ecosystem ^{13}C assimilated (above + belowground ^{13}C content) at the 4-week sampling time was statistically indistinguishable from the belowground assimilated ^{13}C at the 6-month sampling time. Root growth of annual species characteristic of these systems has been shown to decline by March (Jackson et al., 1989), suggesting that the ^{13}C recovered in the belowground pool at the 4-week sampling time may have been primarily composed of structural plant root compounds. Additionally, under typical rainfall conditions, soil respiration in California annual grasslands has been shown to greatly decline by early April (Eviner, 2001), as sources of labile C substrates dwindle, and soil moisture begins to decline. This could explain why we saw little evidence of late growing-season decomposition or loss of ^{13}C. ^{13}C recovery in the belowground pool at our 6-month sampling time was 64% of the total ^{13}C present immediately following the labeling period. Other studies in California annual grassland ecosystems have described similarly high accumulations of C (Schaeffer et al., 2017), and added ^{13}C (Castanha et al., 2018) over the summer dry period. This appears to occur because of the large C input as dead root litter (following annual plant senescence and death in June-July each year), and the reduced ability of microbes to access and decompose this C due to the very low soil moisture characteristic of the Mediterranean-type summer; desiccation results in very low activity of decomposers as well as physical isolation from C substrates (Blankinship & Schimel, 2018).

4.2 Soil density fractions

In our study, the vast majority of soil organic carbon was recovered in the HF pool. We assume the heavy fraction is primarily composed of mineral-associated organic matter (MAOM), i.e. organic matter stabilized via mineral sorption and co-precipitation mechanisms (Kogel-Knabner et al., 2008). Mineral-associated SOM generally has a C:N ratio that aligns with the

C:N ratio of microbes (~10), as opposed to living plant material (>20), (Clemente et al., 2011). The C:N ratio of the HF in our study was consistently near 9:1, suggesting this HF carbon is largely of microbial origin. It has been shown that microbial products are more efficiently and effectively adsorbed to and thus stabilized by soil minerals than are plant-derived compounds (Lavallee et al., 2019). Furthermore, microbial transformation of detrital carbon inputs has been shown to be a critical precursor to long-term carbon stabilization (Cotrufo et al., 2013).

The C:N ratios of the FLF and OLF were approximately 20:1 and 17.5:1 respectively, reflecting a more plant-like signature than the HF material, and the C:N ratio of the OLF was consistently slightly lower than that of the FLF. As well, we found slightly higher total carbon in the OLF than in the FLF. California annual grasslands are typically dominated by annual herbaceous plant communities whose litter decomposes completely within three years (Eviner & Firestone, 2007), resulting in minimal FLF accumulation compared to other ecosystems (Crow et al., 2007). C-rich fungal hyphae, bacterial EPS, and plant mucilage promote soil aggregation both as physical structuring agents as well as major contributors to aggregate-associated soil carbon (Six et al. 2004). OLF material has been found to be largely dominated by fine root fragments and fungal hyphae (Kakouridis et al., 2021). The intermediate OLF C:N ratio we measured (between that of FLF and HF) suggests that microbial constituents and aggregation mechanisms such as fungal hyphae and bacterial EPS may have contributed to OLF formation in our samples, although extensive microbial processing of OLF material is likely limited due to physical protection mechanisms. If we interpret C:N ratios as an indicator of decomposition, then our data suggests increasing decomposition progressing from FLF to OLF to HF (Hyvonen et al., 1996).

The source compounds of ^{13}C recovered in the density fractions likely differs by season. ^{13}C recovered from Spring18-harvested soil likely represent mostly rhizodeposits and labile carbon substrates exuded by roots and possibly consumed by root-associated bacteria and fungi as well as AMF-mediated carbon flow from $^{13}CO_2$-labeled plants (Kakouridis et al., 2021). By our Fall18 sampling, which occurred at the end of the summer dry period, much of the ^{13}C in FLF would have been composed of senesced/dead $^{13}CO_2$- labeled root detritus; we assume that most of the ^{13}C in the HF and OLF was root-derived (Jackson et al., 2017). The onset of the 2018-2019 growing season (due to fall and winter rainfall), likely triggered decomposition of this senesced ^{13}C- labeled shoot material derived from the previous growing season. Some of this decomposing ^{13}C-labeled material could have been incorporated into the soil, representing an additional potential ^{13}C source by the Spring19 sampling time. By Spring20 we assume that ^{13}C recovered in the soil density fractions largely represents soil organic carbon that persisted from Spring19.

^{13}C-SOC was recovered in all three density fractions at 4 weeks, 6 months, 1 year, and 2 years after ^{13}C labeling (Figure 3). We observed a conspicuous increase in FLF ^{13}C content between 4-weeks and 6-months sampling times due to rapid incorporation of ^{13}C-labeled root detritus into this fraction following plant senescence and death, as well as likely incorporation of some aboveground litter; however, an equally conspicuous decrease in ^{13}C within this fraction was observed between 6 months and 1 year after ^{13}C labeling. Between the Fall of 2018 and Spring of 2019, about 38% of FLF material was either converted into more protected forms or lost as CO_2. Such seasonal transience was not as apparent in the OLF or HF.

Additionally, of the three fractions, ^{13}C enrichment was generally lowest in the OLF, indicating that this fraction is not as dynamic as the FLF, or perhaps even as the HF. This could

suggest that the incorporation of "new" carbon into soil aggregates occurs less rapidly than does association of this carbon with minerals, or that stable aggregate formation requires repeated iterations of certain environmental conditions, such as annual plant growth periods or seasonal wet-dry cycles, the extent of which were not captured in the timespan of this study (Totsche et al., 2018). However, over this 2-year study, we see the distribution of ^{13}C among the density fractions approaching that of total C; it is likely that with additional time, the quantity of ^{13}C remaining in the OLF will exceed that remaining in the FLF (Figure 3).

The rapid association of rhizosphere-derived carbon with mineral surfaces was also observed by *Neurath et al. 2021,* in similar soils, who characterized the short-term dynamics (3 months) of root-input carbon. In that study, over the course of a 2-month incubation, the flux of new carbon onto and off of the mineral surfaces was substantial (accounting for over 6% of total C) while total mineral-associated C remained constant. For our study, this finding implies that some of the HF association with ^{13}C OM could in fact be more dynamic than what we observed. By our two-year sampling, 77% of initial ^{13}C stock had been lost from the system. However, of the carbon remaining, over 50% was in a protected form (occluded within soil microaggregates or associated with soil minerals) (Table 2). Furthermore, by four weeks after ^{13}C labeling, we recovered 61% of soil ^{13}C in the HF (Table 2), and quantity of ^{13}C recovered in HF material did not detectably decline over the course of the study. This observation supports the importance of root and rhizosphere-derived carbon inputs in SOM formation (Sokol & Bradford, 2019; Pett-Ridge & Firestone, 2017), and is consistent with rapid microbially-mediated stabilization of carbon onto mineral surfaces (Kallenbach et al., 2016).

Our work indicates that initial associations between minerals and root-derived organic matter are significant and form rapidly. While the majority of annual C inputs to soil cycle

513 rapidly (<2-year timescale), a sizeable proportion (11.5% original ^{13}C inputs persist in HF by
514 year 2) can potentially persist longer. In a study modeling soil carbon turnover in a California
515 grassland site with similar physical characteristics to ours, Torn et al. (2013) calculated that 7%
516 of HF carbon sampled from the 1-15cm depth was "fast" cycling (<2 year turnover) and 93%
517 cycled on a centennial timescale. Our observations provide support for the existence of this small
518 yet rapidly cycling HF carbon pool, but also suggest that the HF does not represent a single C
519 pool operating on a single timescale, but rather multiple pools operating on multiple timescales
520 (Lehmann & Kleber, 2015).

521 **4.3 ^{13}C NMR on heavy fraction**

522 The combination of techniques used in this study provides a window into the dynamics
523 and chemical characteristics of MAOM formation. The labeling of field plots with $^{13}CO_2$ with
524 subsequent sampling and soil density fractionation allowed us to trace the flow and fate of plant-
525 derived inputs into organo-mineral associations. By applying ^{13}C CPMAS NMR spectroscopy to
526 our ^{13}C labeled heavy fraction samples, we sought to further resolve the chemistry of "new"
527 plant-derived carbon in the heavy fraction.

528 It is generally accepted that microbial products are a dominant source of mineral-
529 stabilized organic matter that builds up in heavy fraction material over time (Preston et al., 2009;
530 Creamer et al., 2019). The alkyl C functional group may represent a variety of microbial and
531 plant-derived aliphatic compounds such as lipids, proteins, and waxes (Kögel-Knabner, 1997). In
532 fact, in HF material isolated from a similar site at HREC, Neurath et al. found mineral-associated
533 lipids were largely microbially derived (Neurath et al., 2021). Peaks in the O-Alkyl C region may
534 represent various carbohydrates, proteins, and amino acids (Mathers et al., 2007), including

plant-derived carbohydrates such as cellulose and hemicellulose (Kögel-Knabner, 1997), as well as N-rich proteins and root-exudate derived sugars (Angst et al., 2018). However, O-Alkyl C proportions in HF samples have also been attributed to carbohydrates of microbial origin (Schöning et al., 2006). The aromatic C functional group can contain plant-derived phenolic compounds such as lignin and tannins, aromatic portions of proteins and amino acids, as well as condensed, chemically resistant "black carbon" derived from historically frequent wildfires that occurred in California annual grasslands (Sanderman et al., 2008; Czimczik & Masiello, 2007). The carboxyl C functional group has been described to encompass highly oxidized C forms such as organic acids, ketones, and aldehydes (Mathers et al., 2007), and can be used as an indicator of microbial processing (Ng et al., 2014).

^{13}C NMR spectra are only sensitive to molecules containing ^{13}C. In Spring, 2018, we introduced ^{13}C into the soil. The NMR spectra of the mineral-associated samples collected over the following two years show a decline in the proportion of ^{13}C in the alkyl C functional group, and an increase in the proportion of ^{13}C in the carboxyl C, aromatic C, and carboxyl C functional groups. The relatively constant quantity of ^{13}C present in the HF over the course of the study suggests that alkyl ^{13}C is being converted to carboxyl ^{13}C, or that perhaps, that a portion of HF ^{13}C is transient as suggested by Neurath et al., (2021), and that over the course of our study, some alkyl ^{13}C is lost and some carboxyl ^{13}C is accumulated. Carboxyl C content can be indicative of highly oxidized organic matter (Kogel-Knabner et al., 2008). As such, the increase in the relative proportion of carboxyl C we see over the 2-year study period could have resulted from the oxidation of organic matter during the process of decomposition (Baldock et al., 1992). The fact that we see a higher proportion of alkyl C shortly after the $^{13}CO_2$ labeling period than we do two years later suggests that rhizodeposit C is a substantial source of rapidly forming

558 mineral-alkyl C associations, whether as plant waxes such as cutin, or microbial lipids as
559 suggested by Neurath et al., (2021).

560 Within a two-year period, we see an evolution of the effect of newly introduced ^{13}C on
561 the ^{13}C NMR spectra of the heavy fraction (Figure 4). We expect that some of the added ^{13}C in
562 this fraction underwent chemical transformations during this period and that over time, only the
563 most persistent ^{13}C-HF associations will be retained as less persistent associations disappear.
564 This could leave a legacy of the added ^{13}C label that persists for decades or even centuries
565 (Baisden et al., 2002), while the overall effect of the added ^{13}C label should decline over time.

566 **5. Conclusion and future directions**

567 Understanding the patterns and control of soil organic carbon cycling in California annual
568 grasslands is a critical precursor to any soil carbon management efforts within these ecosystems.
569 Our study traced soil organic carbon formation from plant photosynthesis through its movement
570 into and between soil fractions—and chemical forms in the heavy fraction—for two years. By
571 applying a combination of analytical and spectroscopic techniques, we followed plant carbon
572 from living roots to root detritus to occluded carbon and mineral-associated pools. About a
573 quarter of the C fixed during the 5-day labeling was still present two years after the labeling;
574 most of that "2-year old" carbon was found in the mineral associated heavy fraction. Solid-state
575 ^{13}C NMR spectroscopy was sufficiently sensitive to the ^{13}C introduced that we were able to
576 detect the photosynthetically derived carbon movement into and through the components of the
577 mineral-associated carbon pool. This "new" carbon appears to have a distinct chemical
578 fingerprint from the total background C; that spectroscopic profile declines over the 2 years in
579 the field.

580 ^{13}C analysis and ^{13}C NMR both revealed that the movement of carbon into the heavy
581 fraction occurred rapidly in our system, within four weeks of plant photosynthesis, and that the
582 influence of this "new" carbon on the total background C persisted over the course of our study.
583 Future research that distinguishes between the labile vs. litter inputs on stabilized soil organic
584 carbon formation, and that tracks those dynamics over decadal timescales, would further resolve
585 how plant community characteristics (plant growth stage, lifecycle, seasonal climate parameters)
586 influence the accrual and persistence of soil organic carbon and help us to better predict the
587 responsiveness of annual grassland ecosystems to soil carbon management.

588

589 ## Acknowledgements

590 This research was supported by the US Department of Energy (DOE) Office of Science, Office
591 of Biological and Environmental Research Genomic Science program under award DE-
592 SC0016247 (to MKF) and awards SCW1589, SCW1421 and the LLNL Soil Microbiome SFA,
593 SCW1632 (to JPR). Work conducted at Lawrence Livermore National Laboratory was supported
594 under the auspices of the U.S. DOE under Contract DE-AC52-07NA27344. Work conducted at
595 Lawrence Berkeley National Laboratory was supported under Contract DE-AC02-05CH11231.
596 Soil and plant collection and field plot management was supported by the Hopland Research and
597 Extension Center.

598 ## 5. Citations

599 Angst, G., Messinger, J., Greiner, M., Häusler, W., Hertel, D., Kirfel, K., ... Mueller, C. W.
600 (2018). Soil organic carbon stocks in topsoil and subsoil controlled by parent material,

carbon input in the rhizosphere, and microbial-derived compounds. Soil Biology and Biochemistry, 122, 19–30. https://doi.org/10.1016/j.soilbio.2018.03.026

Angst, G., Mueller, K. E., Klass, G. J. N., Simpson, M. J. (2021). Plant- or microbial-derived? A review on the molecular composition of stabilized soil organic matter. Soil Biology and Biochemistry, 156. https://doi.org/10.1016/j.soilbio.2021.108189

AOAC Official Method 972.43, Microchemical Determination of Carbon, Hydrogen, and Nitrogen, Automated Method, in Official Methods of Analysis of AOAC International, 16th Edition (1997), Chapter 12, pp. 5-6, AOAC International, Arlington, VA.

Bailey, V. L., Pries, C. H., & Lajtha, K. (2019). What do we know about soil carbon destabilization? Environmental Research Letters, 14(8), 083004. https://doi.org/10.1088/1748-9326/ab2c11

Baker, S. E., Peridas, G., Stolaroff, J. K., Goldstein, H. M., Pang, S. H., Lucci, F. R., Li, W., Slessarev, E. W., Pett-Ridge, J., Ryerson, F. R., and Aines, R. D., (2019). Getting to Neutral: Options for Negative Carbon Emissions in California (No. LLNL-TR-796100). Lawrence Livermore National Laboratory (LLNL), Livermore, CA (United States).

Baisden, W. T., Amundson, R., Cook, A. C., & Brenner, D. L. (2002). Turnover and storage of C and N in five density fractions from California annual grassland surface soils. Global Biogeochemical Cycles, 16(4), 64–1. https://doi.org/10.1029/2001gb001822

Bakker, E.; Hubert, F.; Wander, M.M.; Lanson, B. Soil Development under Continuous Agriculture at the Morrow Plots Experimental Fields from X-ray Diffraction Profile Modelling. Soil Syst. 2018, 2, 46. https://doi.org/10.3390/soilsystems2030046

622 Baldock, J. A., Oades, J. M., Waters, A. G., Peng, X., Vassallo, A. M., Wilson, M. A. (1992).
623 Aspects of the chemical structure of soil organic materials as revealed by solid-state ^{13}C
624 NMR spectroscopy. Biogeochemistry, 16(1), 1-42.

625 Barnard, R., Blazewicz, S., and Firestone, M. (2020). Rewetting of soil: revisiting the origin of
626
627 soil CO2 emissions. Soil Biol Biochem. https://doi.org/10.1016/j.soilbio.2020.107819
628
629 Barnard, R. L., Osborne, C. A., & Firestone, M. K. (2013). Responses of soil bacterial and fungal
630 communities to extreme desiccation and rewetting. The ISME Journal, 7(11), 2229-2241.
631 https://doi.org/10.1038/ismej.2013.104

632 Bartolome, J. W., J. Barry, T. Griggs, and P. Hopkinson. (2007). Valley Grasslands. M. G.
633 Barbour, T. Keeler-Wolf, and A. A. Schoenherr (Ed.), *Terrestrial Vegetation of*
634 *California* (pp. 367-393). University of California Press, Berkeley, California.

635 Becchetti, T., George, M., et al. (2016). Rangeland Management Series: Annual Range Forage
636 Production. University of California ANR Publication 8018, 1-12.

637 Biggs, N. B., Huntsinger, L. (2021). Managed grazing on California annual rangelands in the
638 context of state climate policy. Rangeland Ecology and Management, 76(1), 56-68.
639 https://doi.org/10.1016/j.rama.2021.01.007

640 Birch, H. F. (1958). The Effect of soil drying on humus decomposition and nitrogen availability.
641 Plant and Soil, 10(1), 9-31. https://doi.org/10.1007/bf01343734

642 Blankinship, J., & Schimel, J. (2018). Biotic versus Abiotic Controls on Bioavailable Soil
643 Organic Carbon. Soil Systems, 2(1), 10. https://doi.org/10.3390/soilsystems2010010

644 Blazewicz, S. J., Hungate, B. A., Koch, B. J., Nuccio, E. E., Morrissey, E., Brodie, E. L., …
645 Firestone, M. K. (2020). Taxon-specific microbial growth and mortality patterns reveal

distinct temporal population responses to rewetting in a California grassland soil. The ISME Journal. https://doi.org/10.1038/s41396-020-0617-3

Bradford, M. A., Carey, C. J., Atwood, L., Bossio, D., Fenichel, E. P., Gennet, S., ... Wood, S. A. (2019). Soil carbon science for policy and practice. Nature Sustainability, 2(12), 1070–1072. https://doi.org/10.1038/s41893-019-0431-y

Castanha, C., Zhu, B., Hicks Pries, C. E., Georgiou, K., Torn, M. S. (2018). The effects of heating, rhizosphere, and depth on root litter decomposition are mediated by soil moisture. Biogeochemistry, 137(1), 267-279. https://doi.org/10.1007/s10533-017-0418-6

Chou, W. W., Silver, W. L., Jackson, R. D., Thompson, A. W., & Allen-Diaz, B. (2008). The sensitivity of annual grassland carbon cycling to the quantity and timing of rainfall. Global Change Biology, 14(6), 1382-1394. https://doi.org.10.1111/j.1365-2486.2008.01572.x

Clemente, J. S., Simpson, A. J., & Simpson, M. J. (2011). Association of specific organic matter compounds in size fractions of soils under different environmental controls. Organic Geochemistry, 42(10), 1169–1180. https://doi.org/10.1016/j.orggeochem.2011.08.010

Cotrufo, M. F., Wallenstein, M. D., Boot, C. M., Denef, K., & Paul, E. (2013). The Microbial Efficiency-Matrix Stabilization (MEMS) framework integrates plant litter decomposition with soil organic matter stabilization: do labile plant inputs form stable soil organic matter? Global Change Biology, 19(4), 988–995. https://doi.org/10.1111/gcb.12113

Cotrufo, M. F., Soong, J. L., Horton, A. J. Campbell, E. E., Haddix, M. L., Wall, D. H., & Parton, W. J. (2015) Formation of soil organic matter via biochemical and physical pathways of litter mass lost. Nature Geoscience, 8(10), 776-779. https://doi.org/10.1038/ngeo2520

669 Cotrufo, M. F., Ranalli, M. G., Haddix, M. L., Six, J., & Lugato, E. (2019). Soil carbon storage
670 informed by particulate and mineral-associated organic matter. Nature Geoscience,
671 12(12), 989–994. https://doi.org/10.1038/s41561-019-0484-6
672 Creamer, C. A., Foster, A. L., Lawrence, C., McFarland, J., Schulz, M., Waldrop, M. P. (2019).
673 Mineralogy dictates the initial mechanism of microbial necromass association. Geochim
674 Cosmochim Acta, 260, 161-176. https://doi.org/10.1016/j.gca.2019.06.028
675 Crow, S. E., Swanston, C. W., Lajtha, K., Brooks, J. R., Keirstead, H. (2007). Density
676 fractionation of forest soils: methodological questions and interpretation of incubation
677 results and turnover time in an ecosystem context. Biogeochemistry, 85, 69-90.
678 https://doi.org/10.1007/s10533-007-9100-8
679 Czimczik, C. I. & Maseillo, C. A. (2007). Global Biogeochemical Cycles, 21(1), GB3005.
680 https://doi.org/10.1029/2006GB002798
681 Dass, P., Houlton, B. Z., Wang, Y., Warlind, D. (2018). Grasslands may be more resilient carbon
682 sinks than forests in California. Environ. Res. Lett. 13(7). https://doi.org/10.1088/1748-
683 9326/aacb39
684 Doebelin, N.; Kleeberg, R. (2015). Profex: A graphical user interface for the Rietveld refinement
685 program BGMN. J. Appl. Cryst. 48, 1573–1580.
686 Eviner, V. (2001). Linking plant community composition and ecosystem dynamics: interactions
687 of plant traits determine the ecosystem effects of plant species and plant species mixtures.
688 PhD Dissertation. Integrative Biology. The University of California, Berkeley. 404 pp.
689 Eviner, V. T., & Firestone, M. K. (2007). Mechanisms Determining Patterns of Nutrient
690 Dynamics. M. Stromberg, J. Corbin, and C. D'Antonio (Ed.), *California Grasslands:*

691 *Ecology and Management,* (pp. 94-106). University of California Press, Berkeley,
692 California

693 Golchin, A., Oades, J., Skjemstad, J., Clarke, P. (1994). Study of free and occluded particulate
694 organic matter in soils by solid state 13C CP/MAS NMR spectroscopy and scanning
695 electron microscopy. Soil Res. 32, 285-309. https://doi.org/10.1071/SR9940285

696 Heady, H. F., Bartolome, J. W., Pitt, M. D., Savelle, G. D., Stroud, M. C. (1992). California
697 Prairie. Pages 313-335 in R. T. Coupland, editor. Natural Grasslands. Ecosystems of the
698 World 8A. Elsevier, New York, New York.

699 Helfrich, M., Ludwig, B., Buurman, P., & Flessa, H. (2006). Effect of land use on the
700 composition of soil organic matter in density and aggregate fractions as revealed by
701 solid-state ^{13}C NMR spectroscopy. Geoderma, 136(1-2), 331-341.
702 https://doi.org/10.1016/j.geoderma.2006.03.048

703 Hicks Pries, C. E., Bird, J. A., Castanha, C., Hatton, P.-J., & Torn, M. S. (2017). Long term
704 decomposition: the influence of litter type and soil horizon on retention of plant carbon
705 and nitrogen in soils. Biogeochemistry, 134(1–2), 5–16. https://doi.org/10.1007/s10533-
706 017-0345-6

707 Hyvonen, R., Agren, G. I., & Andren, O. (1996). Modelling Long-Term Carbon and Nitrogen
708 Dynamics in an Arable Soil Receiving Organic Matter. Ecological Applications, 6(4),
709 1345–1354. https://doi.org/10.2307/2269612

710 Jackson, L. E., Schimel, J. P., & Firestone, M. K. (1989). Short-term partitioning of ammonium
711 and nitrate between plants and microbes in an annual grassland. Soil Biology and
712 Biochemistry, 21(3), 409-415. https://doi.org/10.1016/0038-0717(89)90152-1

713 Jackson, R. B., Lajtha, K., Crow, S. E., Hugelius, G., Kramer, M. G., & Piñeiro, G. (2017). The
714 Ecology of Soil Carbon: Pools, Vulnerabilities, and Biotic and Abiotic Controls. Annual
715 Review of Ecology, Evolution, and Systematics, 48(1), 419–445.
716 https://doi.org/10.1146/annurev-ecolsys-112414-054234

717 Kakouridis, A., Yuan, M., Hagen, J., Fossum, C., Moore, M., Herman, D., Nico, P., Weber, P.,
718 Pett-Ridge, J., Firestone, M. (2021). AMF transport of plant carbon into soil alters the
719 characteristics of soil organic carbon as well as the soil microbial community. *bio*Rxiv
720 https://doi.org/10.1101/2020.09.21.305409

721 Kallenbach, C. M., Frey, S. D., & Grandy, A. S. (2016). Direct evidence for microbial-derived
722 soil organic matter formation and its ecophysiological controls. Nature Communications,
723 7(1). https://doi.org/10.1038/ncomms13630

724 Kögel-Knabner, I. (1997). ^{13}C and ^{15}N NMR spectroscopy as a tool in soil organic matter
725 studies. Geoderma, 80(1), 243-260.

726 Kögel-Knabner, I., Guggenberger, G., Kleber, M., Kandeler, E., Kalbitz, K., Scheu, S.,
727 Eusterhues, K., Leinweber, P. (2008). Organo-mineral associations in temperate soils:
728 Integrating biology, mineralogy, and organic matter chemistry. Journal of Plant Nutrition
729 and Soil Science, 171(1), 61–82. https://doi.org/10.1002/jpln.200700048

730 Lang, S. Q., Bernasconi, S. M., & Früh-Green, G. L. (2012). Stable isotope analysis of organic
731 carbon in small (µg C) samples and dissolved organic matter using a GasBench
732 preparation device. Rapid Commun. Mass Spectrom, 26(1), 9-16.
733 https://doi.org/10.1002/rcm.5287

734 Lavallee, J. M., Soong, J. L., & Cotrufo, M. F. (2019). Conceptualizing soil organic matter into
735 particulate and mineral-associated forms to address global change in the 21st century.
736 Global Change Biology, 26(1), 261–273. https://doi.org/10.1111/gcb.14859
737 Lehmann, J., & Kleber, M. (2015). The contentious nature of soil organic matter. Nature,
738 528(7580), 60–68. https://doi.org/10.1038/nature16069
739 Mathers, N. J., Jalota, R. K., Dalal, R. C., Boyd, S. E. (2007). ^{13}C-NMR analysis of decomposing
740 litter and fine roots in the semi-arid Mulga Lands of southern Queensland. Soil Biology
741 and Biochemistry, 39(1), 993-1006. https://doi.org/10.1016/j.soilbio.2006.11.009
742 Manzoni, S., & Katul, G. (2014). Invariant soil water potential at zero microbial respiration
743 explained by hydrological discontinuity in dry soils. Geophysical Research Letters,
744 41(20), 7151-7158. https://doi.org/10.1002/2014g1061467
745 Mendiburu, F. D. (2015). Agricolae: statistical procedures for agricultural research. Version 1.2-
746 3. http://CRAN.R-project.org/package=agricolae
747 Neurath, R., Pett-Ridge, J., Chu-Jacoby, I., Herman, D., Whitman, T., Nico, P., Lipton, A. S.,
748 Kyle, J., Tfaily, M. M., Thompson, A., Firestone, M. K. (2021). Root carbon interaction
749 with soil minerals is dynamic, leaving a legacy of microbially-derived residues. bioRxiv.
750 https://doi.org/10.1101/2021.03.23.436628
751 Ng, E.-L., Patti, A. F., Rose, M. T., Schefe, C. R., Wilkinson, K., Smernik, R. J., Cavagnaro, T.
752 R. (2014). Does the chemical nature of soil organic carbon drive the structure and

753 functioning of soil microbial communities? Soil Biology & Biochemistry, 70(1). 54-61.
754 http://dx.doi.org/10.1016/j.soilbio.2013.12.004
755 Pett-Ridge, J., & Firestone, M. K. (2017). Using stable isotopes to explore root-microbe-mineral
756 interactions in soil. Rhizosphere, 3, 244–253.https://doi.org/10.1016/j.rhisph.2017.04.016
757 Pett-Ridge, J., Shi, J., Estera-Molina, K., Nuccio, E. E., Yuan, M., Rijkers, R., Swenson, T.,
758 Zhalnina, K., Northern, T., Zhou, J., Firestone, M. K. (2021). Rhizosphere Carbon
759 Turnover from Cradle to Grave: The Role of Microbe-Plant Interactions. In: Gupta V.,
760 Sharma A. (eds) Rhizosphere Biology: Interactions Between Microbes and Plants.
761 Rhizosphere Biology. Springer, Singapore. https://doi.org/10.1007/978-981-15-6125-2_2.
762 Poeplau, C., Don, A., Six, J., Kaiser, M., Benbi, D., Chenu, C., ... Nieder, R. (2018). Isolating
763 organic carbon fractions with varying turnover rates in temperate agricultural soils – A
764 comprehensive method comparison. Soil Biology and Biochemistry, 125, 10–26.
765 https://doi.org/10.1016/j.soilbio.2018.06.025
766 Preston, C. M., Nault, J. R., & Trofymow, J. A. (2009). Chemical changes during 6 years of
767 decomposition of 11 litter in some Canadian forest sites. Part 2. ^{13}C abundance, solid-
768 state ^{13}C NMR spectroscopy and the meaning of "lignin". Ecosystems, 12(1), 1078-1102.
769 https://doi.org/10.1007/s10021-009-9267-z
770 Sanderman, J., Baldock, J. A., & Amundson, R. (2008). Dissolved organic carbon chemistry and
771 dynamics in contrasting forest and grassland soils. Biogeochemistry, 89(2), 181-198.
772 Schaeffer, S. M., Homyak, P. M., Boot, C. M., Roux-Michollet, D., & Schimel, J. P. (2017). Soil
773 carbon and nitrogen dynamics throughout the summer drought in a California annual
774 grassland. Soil Biology and Biochemistry, 115, 54–62.
775 https://doi.org/10.1016/j.soilbio.2017.08.009

776 Schimel, J. P. (2018). Life in Dry Soils: Effects of Drought on Soil Microbial Communities and
777 Processes. Annual Review of Ecology, Evolution, and Systematics, 49(1), 409-432.
778 https://doi.org/10.1146/annurev-ecolsys-110617-062614
779 Schöning, I. & Kögel-Knabner, I. (2006). Chemical composition of young and old carbon pools
780 throughout Cambisol and Luvisol profiles under forests. Soil Biology and Biochemistry,
781 38(1), 2411-2424. https://doi.org/10.1016/j.soilbio.2006.03.005

782 Sheldrick, B. H. and Wang, C. 1993. Particle-size Distribution. pp. 499-511. In: Carter, M. R.
783 (ed), Soil Sampling and Methods of Analysis, Canadian Society of Soil Science, Lewis
784 Publishers, Ann Arbor, MI.

785 Sher, Y., Baker, N. R., Herman, D., Fossum, C., Hale, L., Zhang, X., ... Firestone, M. (2020).
786 Microbial extracellular polysaccharide production and aggregate stability controlled by
787 switchgrass (Panicum virgatum) root biomass and soil water potential. Soil Biology and
788 Biochemistry, 143, 107742. https://doi.org/10.1016/j.soilbio.2020.107742

789 Singer, M. J., Southard, R. J., Warrington, D. N., & Janitzky, P. (1992). Stability of Synthetic
790 Sand-Clay Aggregates after Wetting and Drying Cycles. Soil Science Society of America
791 Journal, 56(6), 1843–1848. https://doi.org/10.2136/sssaj1992.03615995005600060032x

792 Six, J., Bossuyt, H., Degryze, S., & Denef, K. (2004). A history of research on the link between
793 (micro)aggregates, soil biota, and soil organic matter dynamics. Soil and Tillage
794 Research, 79(1), 7–31. https://doi.org/10.1016/j.still.2004.03.008

795 Soil Survey Staff. Web Soil Survey. Natural Resources Conservation Service, United States
796 Department of Agriculture. Available online June 1, 2020.

Sokol, N. W., Sanderman, J., & Bradford, M. A. (2018). Pathways of mineral-associated soil organic matter formation: Integrating the role of plant carbon source, chemistry, and point of entry. Global Change Biology, 25(1), 12–24. https://doi.org/10.1111/gcb.14482

Sokol, N. W., & Bradford, M. A. (2019). Microbial formation of stable soil carbon is more efficient from belowground than aboveground input. Nature Geoscience, 12(1), 46–53. https://doi.org/10.1038/s41561-018-0258-6

Sollins, P., Kramer, M. G., Swanston, C., Lajtha, K., Filley, T., Aufdenkampe, A. K., ... Bowden, R. D. (2009). Sequential density fractionation across soils of contrasting mineralogy: evidence for both microbial- and mineral-controlled soil organic matter stabilization. Biogeochemistry, 96(1–3), 209–231. https://doi.org/10.1007/s10533-009- 9359-z

Strickland, T. C., & Sollins, P. (1987). Improved Method for Separating Light- and Heavy-Fraction Organic Material from Soil. Soil Science Society of America Journal, 51(5), 1390–1393. https://doi.org/10.2136/sssaj1987.03615995005100050056x

Terrer, C., R. P., Phillips, B. A., Hungate, J. Rosendale, J. Pett-Ridge, M. Craig, K. J. van Groenigen, T. F. Keenan, B. N. Sulman, B. D. Stocker, P. B. Reich, A. F. A. Pellegrini, E. Pendall, H. Zhang, R. D. Evans, Y. Carrillo, J. B. Fisher, R. B. Jackson. (2020). A trade-off between plant and soil carbon under elevated CO_2. Nature 591: 599-603. doi.org/10/1038/s41586-021-03306-8

Torn, M. S., Trumbore, S. E., Chadwick, O. A., Vitousek, P. M., and Hendricks, D. M. (1997). Mineral control of soil organic carbon storage and turnover. Nature, 389(6647), 170-173. https://doi.org/10.1038/38260

818 Torn, M. S., Kleber, M., Zavaleta, E. S., Zhu, B., Field, C. B., Trumbore, S. E. (2013). A dual
819 isotope approach to isolate soil carbon pools of different turnover times. Biogeosciences,
820 10(1), 8067-8081. https://doi.org/10.5194/bg-10-8067-2013
821 Totsche, K. U., Amelung, W., Gerzabek, M. H., Guggenberger, G., Klumpp, E., Knief, C., ...
822 Kögel-Knabner, I. (2017). Microaggregates in soils. Journal of Plant Nutrition and Soil
823 Science, 181(1), 104–136. https://doi.org/10.1002/jpln.201600451
824 Villarino, S. H., Pinto, P., Jackson, R. B., Piñeiro, G. (2021). Plant rhizodeposition: A key factor
825 for soil organic matter formation in stable fractions. Science Advances, 7(16), 1-13.
826 10.1126/sciadv.abd3176
827 Waldrop, M. P., & Firestone, M. K. (2006). Response of Microbial Community Composition and
828 Function to Soil Climate Change. Microbial Ecology, 52(4), 716–724.
829 https://doi.org/10.1007/s00248-006-9103-3
830 Wickham, H. (2016). ggplot2: Elegant Graphics for Data Analysis. Springer-Verlag New York.
831 ISBN 978-3-319-24277-4, https://ggplot2.tidyverse.org
832 Zhou, X., Liu, D., Bu, H., Deng, L., Liu, H., Yuan, P., Du, P., & Song, H. (2018). XRD-based
833 quantitative analysis of clay minerals using reference intensity ratios, mineral intensity
834 factors, Rietveld, and full pattern summation methods: A critical review. Solid Earth
835 Sciences, 3, 16-29. https://doi.org/10.1016/j.sesci.2017.12.002
836

837 ## 6. Figures & Tables

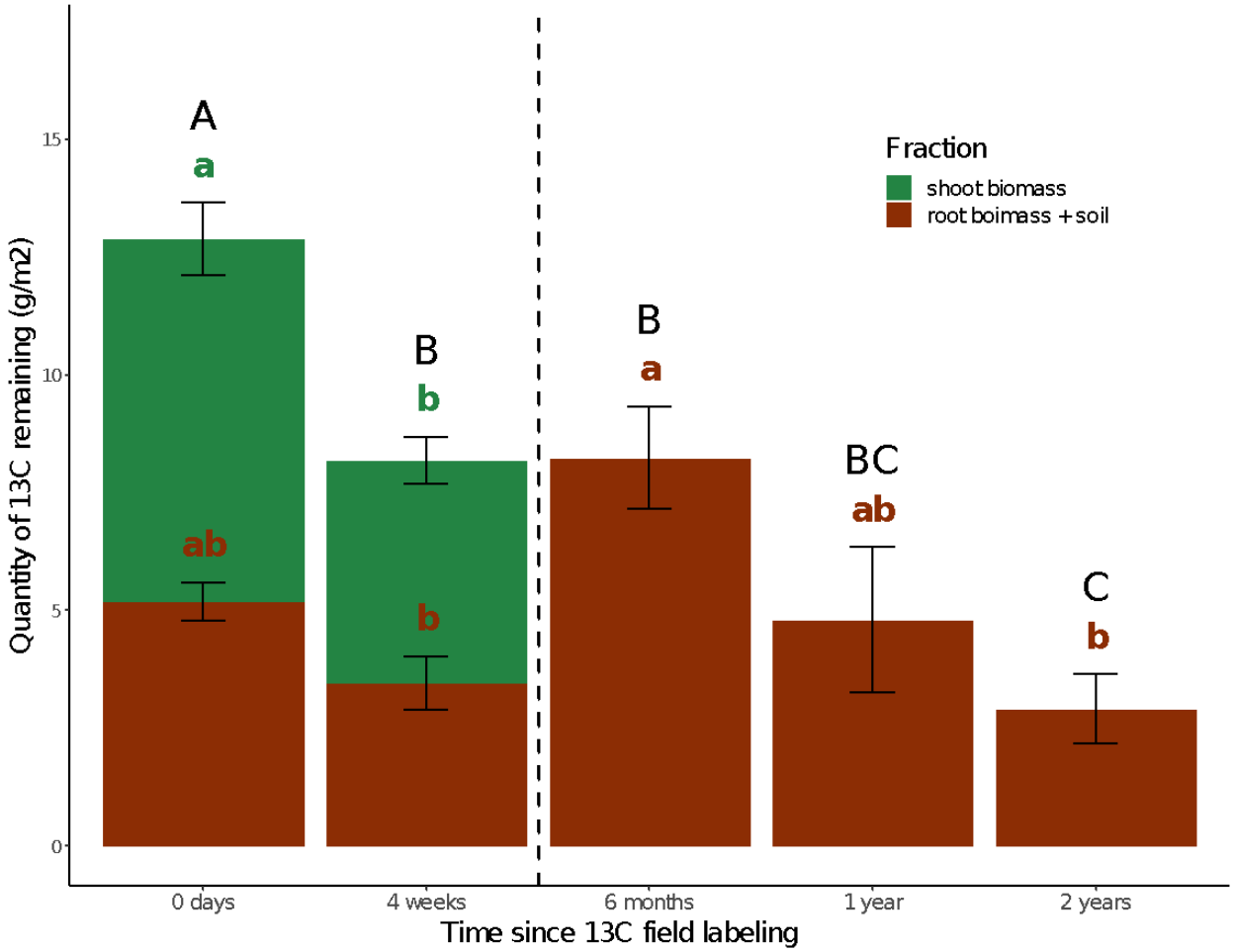

Figure 1. Ecosystem ^{13}C assimilation. Total excess ^{13}C measured in shoot biomass (green) and root biomass + soil (brown). The 0-day timepoint occurred immediately following completion of the 5-day $^{13}CO_2$ labeling. Vertical black dashed line between the 4-weeks and 6-months timepoint marks plant senescence at the end of the spring growing season—hence, no shoot biomass ^{13}C measurements occurred beyond that point and previously living root ^{13}C biomass has become part of the soil ^{13}C. Letters indicate significant differences within a given ecosystem fraction (shoots in green vs. root biomass + soil in brown text), and overall (in black text) between timepoints by Tukey's HSD (p-value = 0.05). Error bars represent 1 SE.

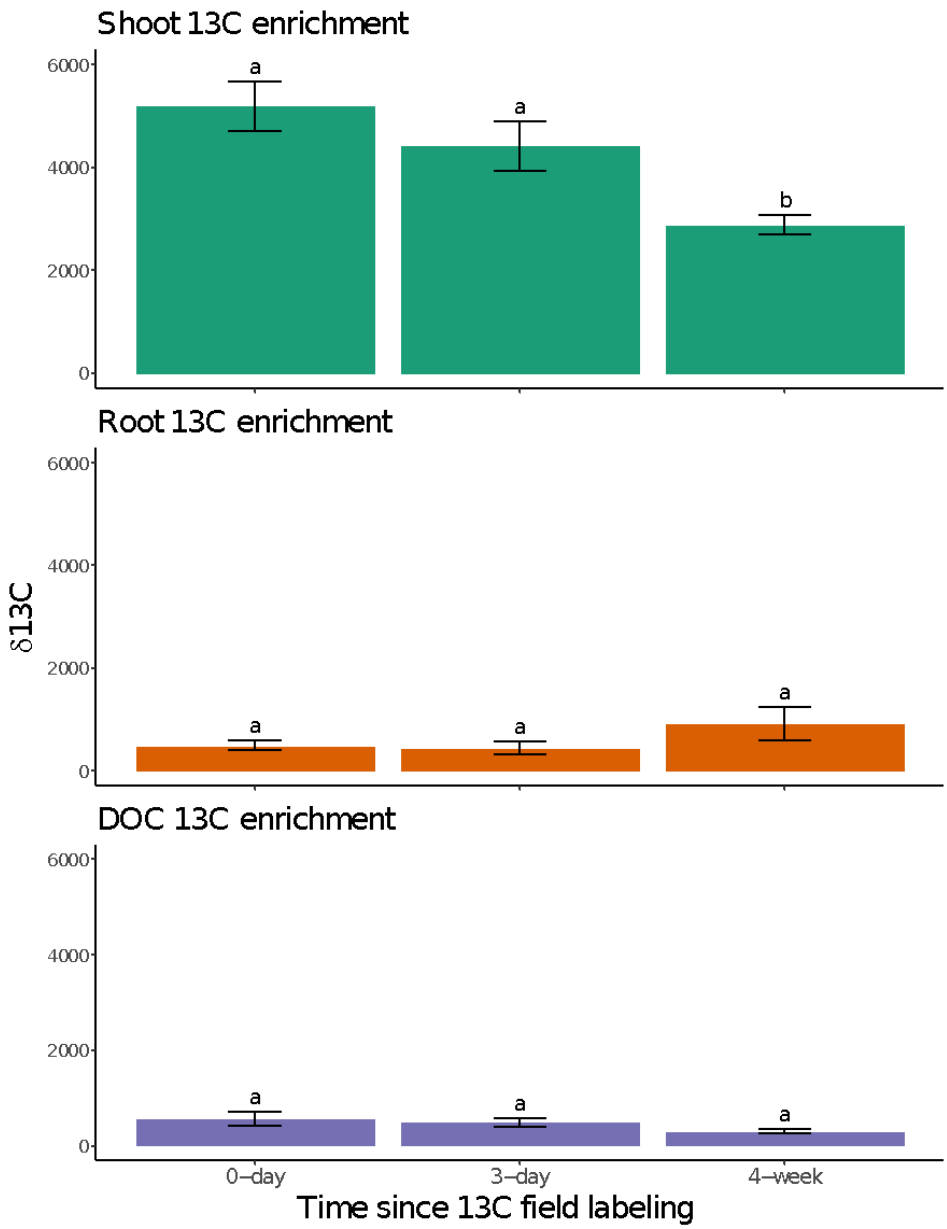

Figure 2. Short-term ecosystem ^{13}C dynamics. Delta ^{13}C values measured in shoot biomass (top), root biomass (middle), and soil DOC (bottom). Timepoints correspond to 0 days, 3 days, and 4 weeks following the completion of the 5-day $^{13}CO_2$ field labeling. Letters indicate significant differences within a given ecosystem fraction (aboveground biomass, roots, DOC) between timepoints by Tukey's HSD (p-value = 0.05). Error bars represent 1 SE.

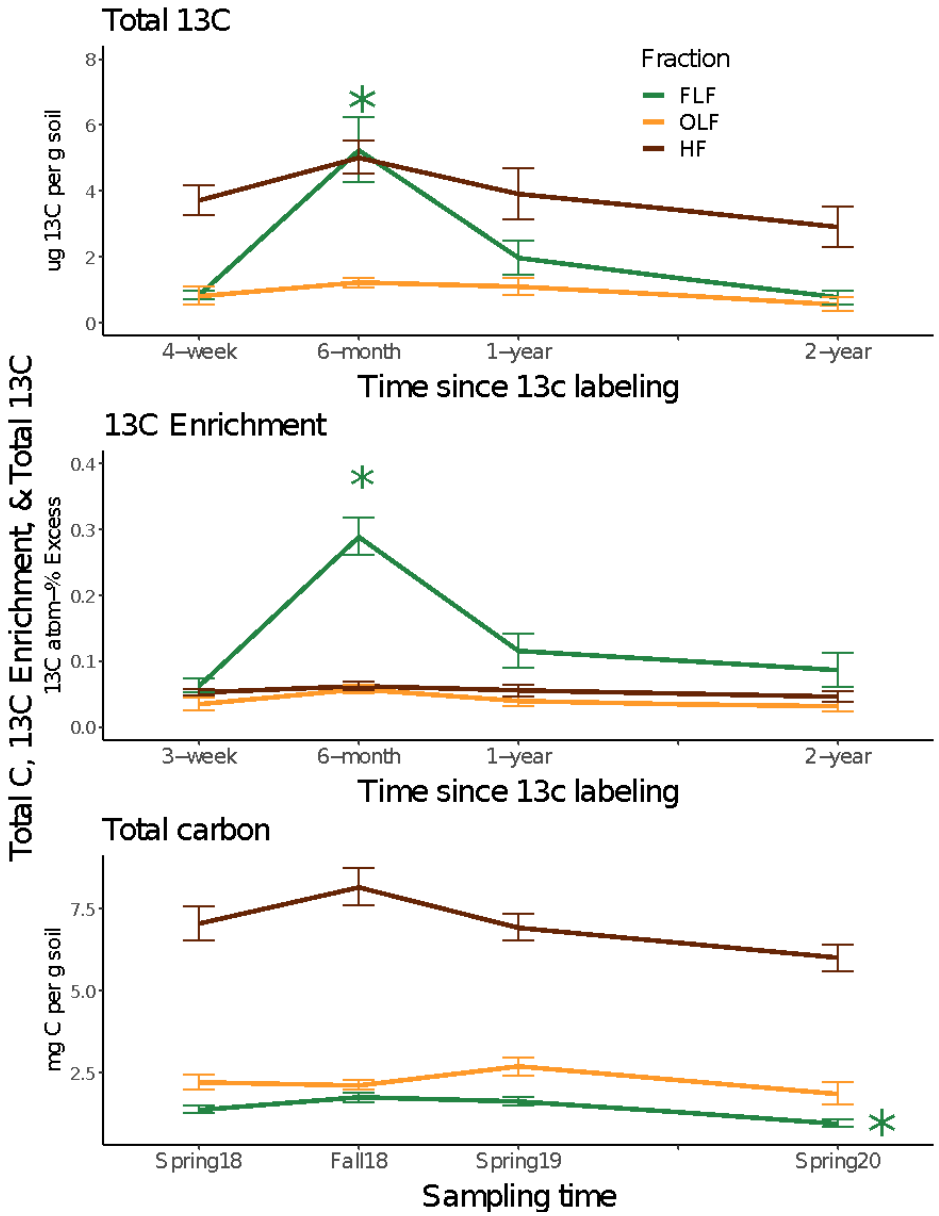

Figure 3. Total ^{13}C, ^{13}C enrichment, and total C distribution among soil density fractions. Total ^{13}C (ug / g soil), ^{13}C enrichment (atom-% excess), and total carbon (mg / g soil) measured for soil density fractions: free-light fraction (FLF), occluded-light fraction (OLF), and heavy fraction (HF). Soil density fractions were determined in Spring18, Fall18, Spring19, and Spring20. These sampling times correspond to 4-weeks, 6-months, 1-year, and 2-years following the $^{13}CO_2$ field labeling. Error bars represent 1 SE. Significant differences by Tukey's HSD (p-value = 0.05) between times are indicated by stars with color coordinating to respective soil density fraction.

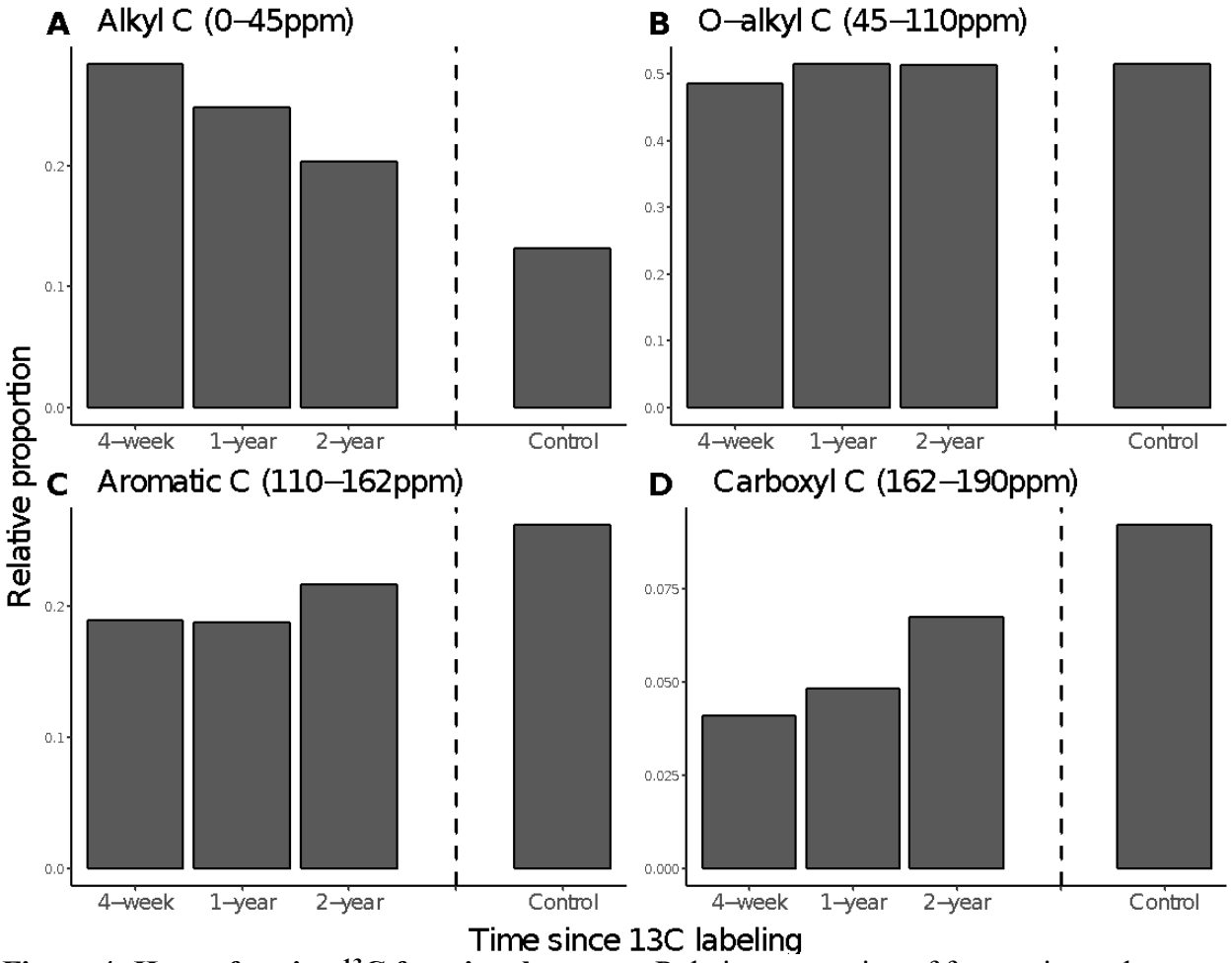

Figure 4: Heavy fraction ^{13}C functional groups. Relative proportion of four major carbon functional groups in heavy fraction separated from soil calculated from ^{13}C NMR spectra. Proportions were calculated by integrating functional group regions A. alkyl C, B. O-alkyl C, C. aromatic C, and D. carboxyl C using Topspin software, and analyzed separately for each spectrum. X axis refers to spectra obtained for ^{13}C-labeled Heavy Fraction soil 4 weeks, 1 year, and 2 years following the ^{13}C-labeling, as well as a ^{12}C-labeled control sample collected in the Spring of 2018. Atom percent ^{13}C for the 4 samples (4-wk, 1 year, 2 years, and control) was 1.145, 1.139, 1.133, and 1.076 respectively.

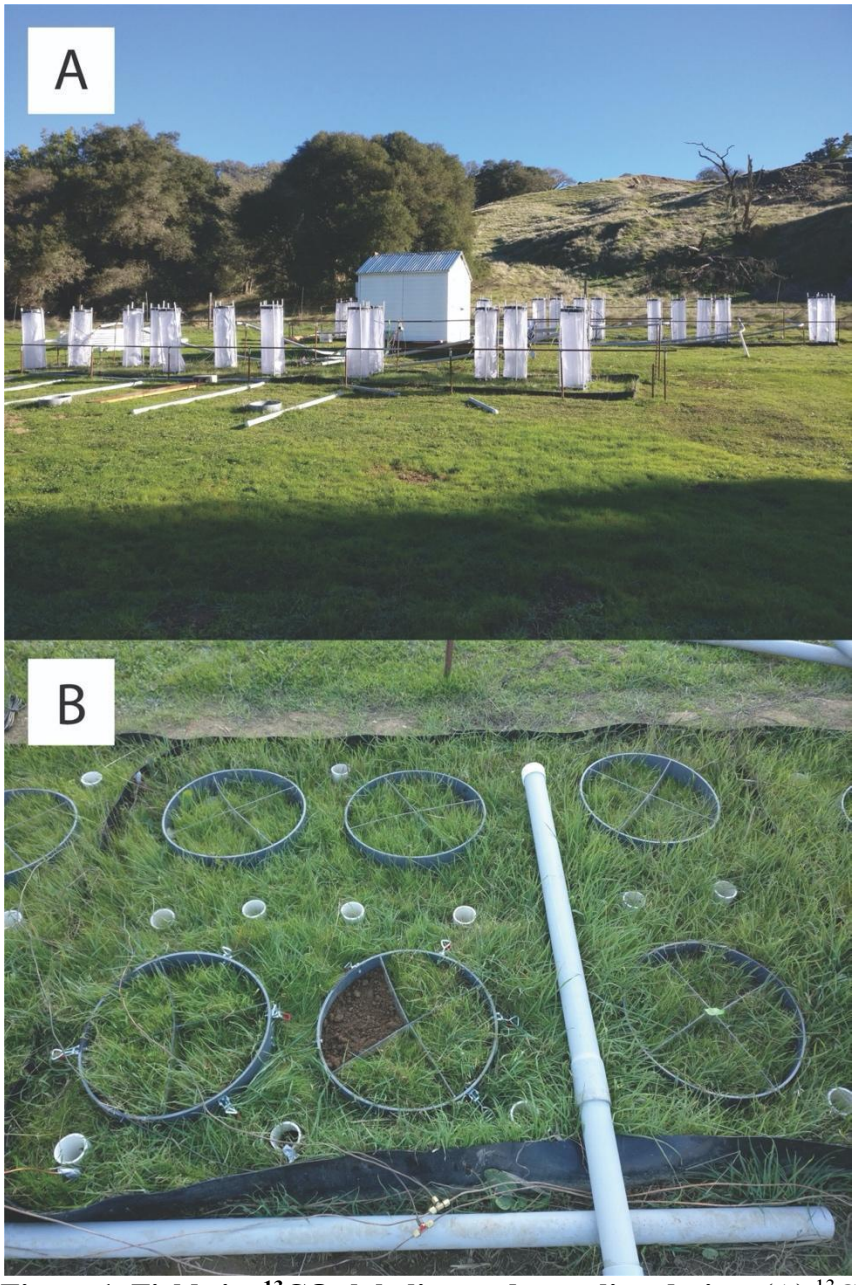

Supplemental Figure 1. Field site $^{13}CO_2$ labeling and sampling design. (A) $^{13}CO_2$ labeling chambers, (B) Field plot with 6 circular subplots; subplots divided into 4 "wedges" for destructive sampling—ex. Bottom row center.

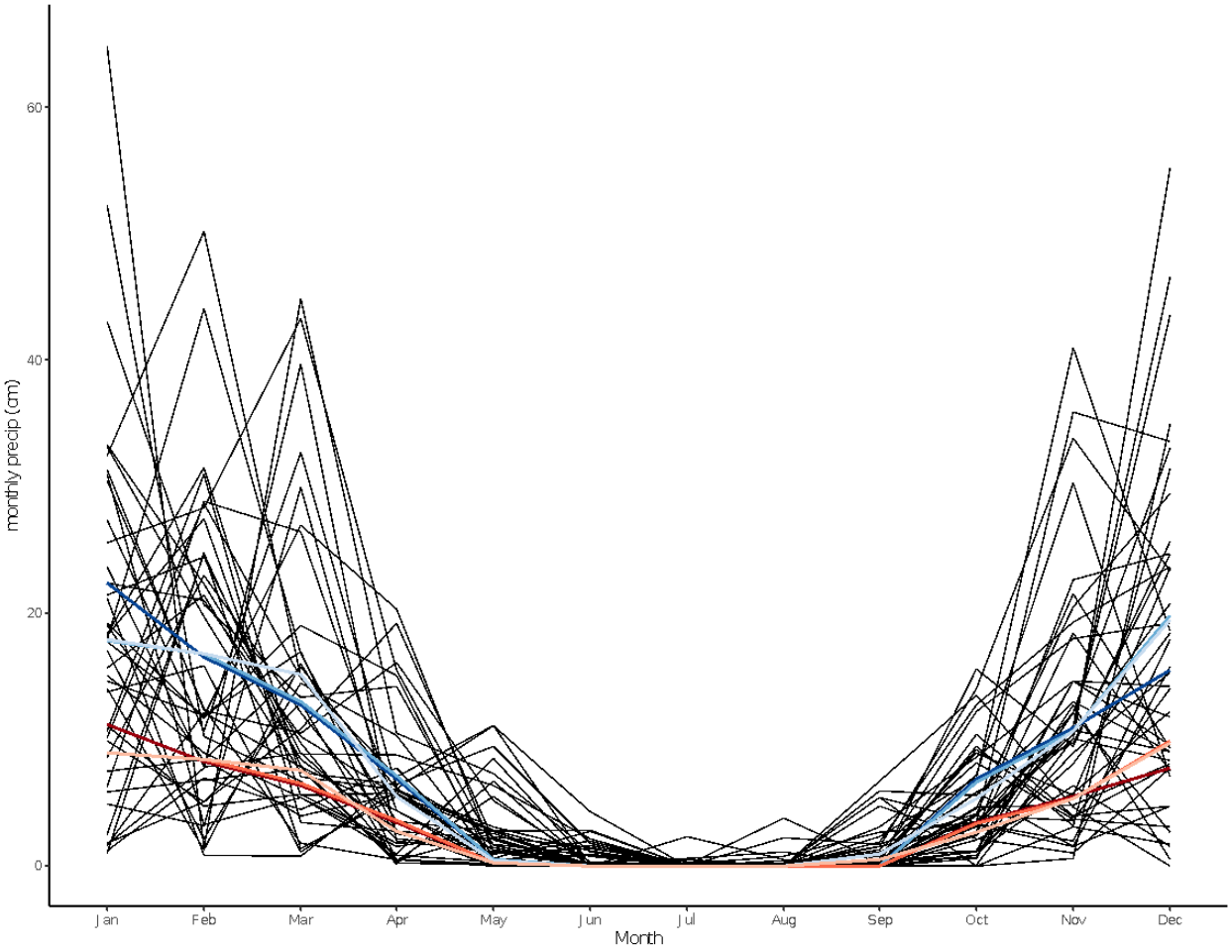

Supplemental Figure 2. 50-year annual precipitation + Annual rainfall for 50% and 100% precipitation treatment plots for 2017-2018, 2018-2019, and 2019-2020 growing seasons. Black lines indicate monthly precipitation at Hopland Research and Extension Center (HREC), our study site, dating back to 1970. Blue lines indicate manipulated rainfall received by our 100% of average annual precipitation treatment plots and red lines indicate manipulated rainfall received by our 50% of average annual precipitation treatment plots. Color shade scales from dark light with darkest blues and reds corresponding to the 2017-2018 growing season, and lightest shades corresponding to the 2019-2020 growing season.

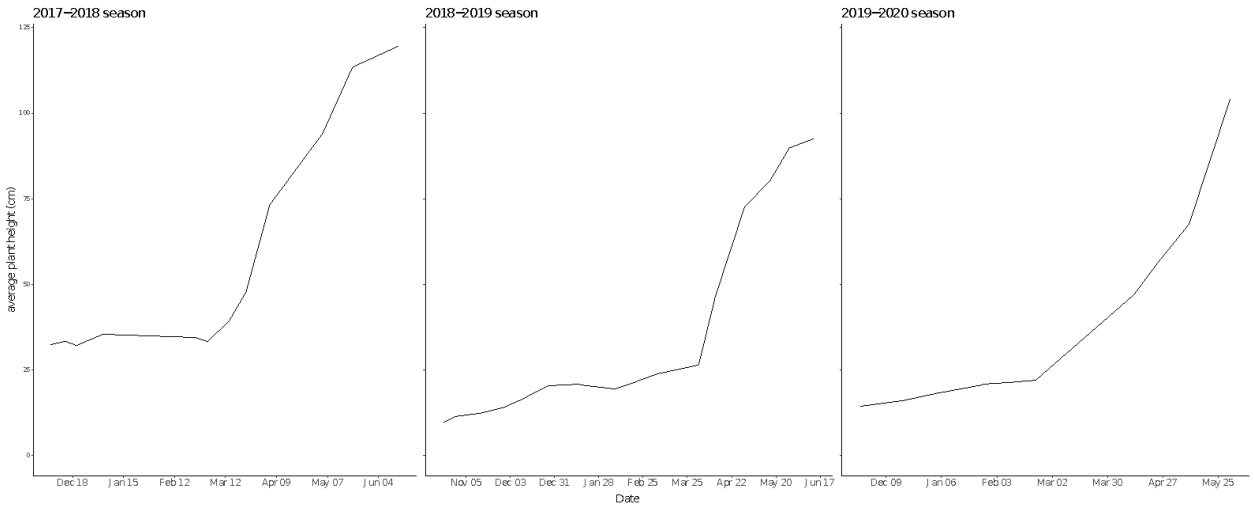

Supplement Figure 3. Average plant heights per season. Lines represent average maximum plant height throughout the three growing seasons. Maximum plant height was measured for each plot (n=16) and was measured in cm.

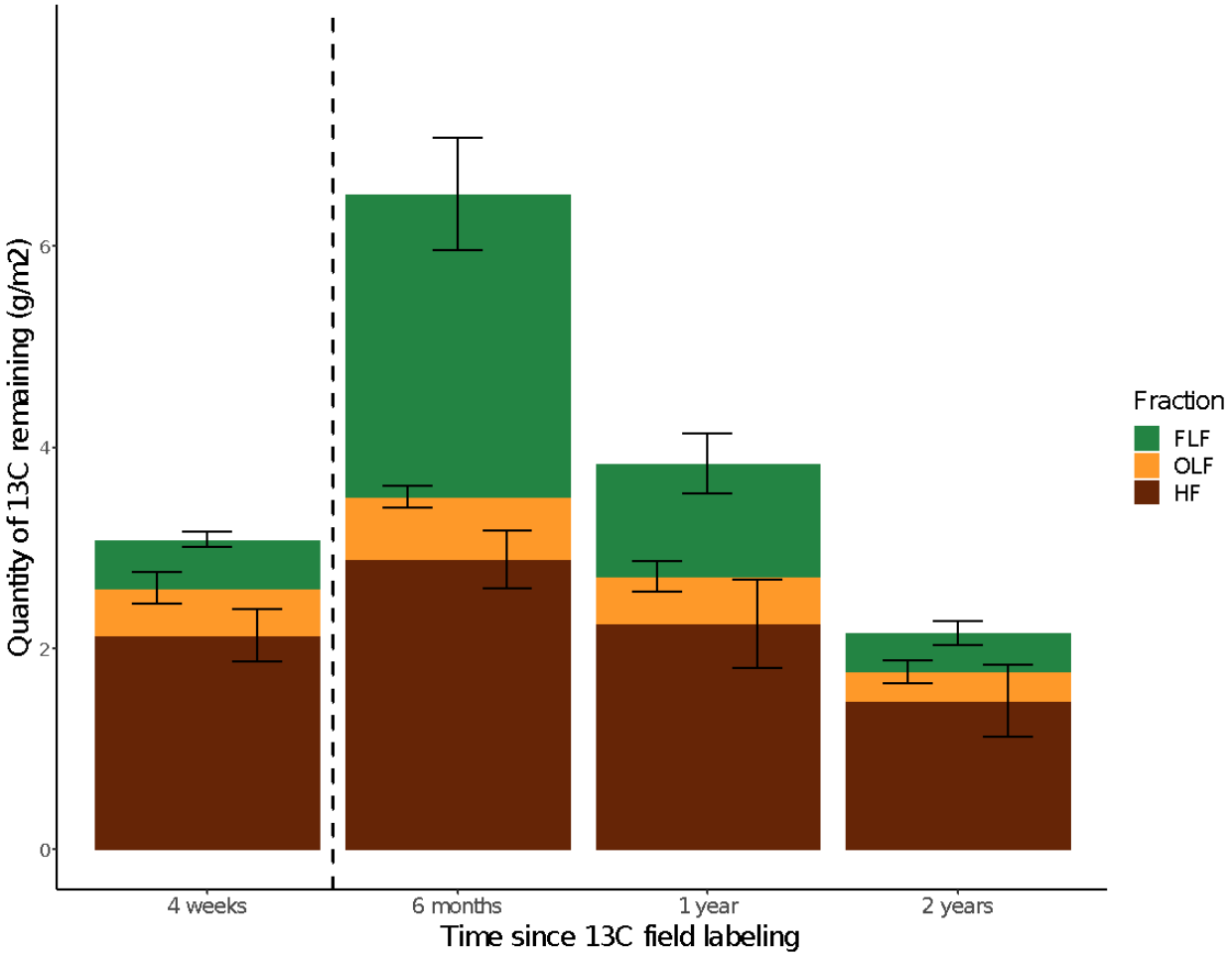

Supplemental Figure 4. ^{13}C assimilation among soil density fractions. Total excess ^{13}C content of soil density fractions: free-light fraction (FLF); occluded-light fraction (OLF) and heavy fraction (HF), scaled to soil volume (15cm sampling depth). Error bars represent 1 SE.

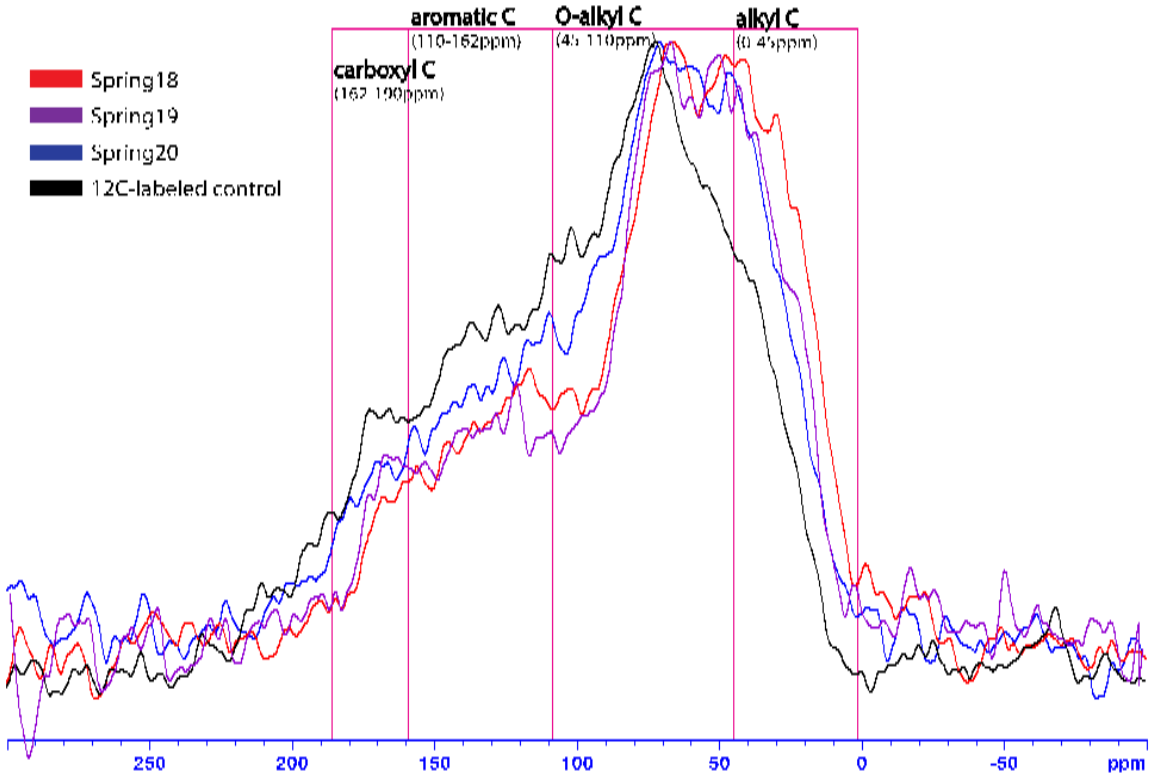

928
929 **Supplemental Figure 5. ^{13}C CPMAS NMR Spectra on Heavy Fraction 4 weeks, 1 year, and**
930 **2 years after ^{13}C labeling relative to control sample.** ^{13}C NMR spectra of heavy fraction soil
931 collected in Spring18 (4 weeks after ^{13}C field labeling), Spring19 (1 year after), Spring20 (2
932 years after), and a ^{12}C-labeleled control (collected in Spring18). Carbon functional groups
933 outlined in pink.
934

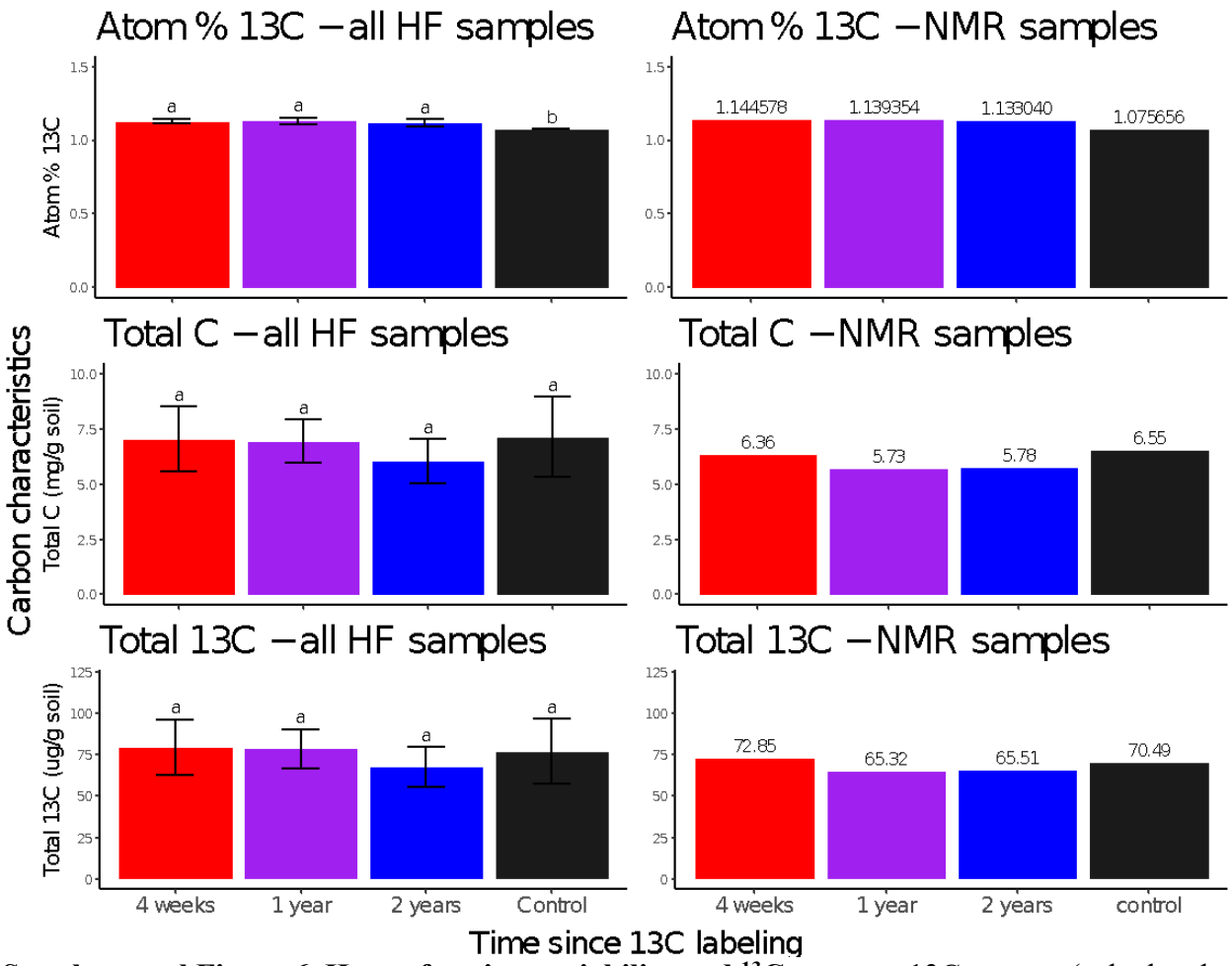

Supplemental Figure 6. Heavy fraction variability and ^{13}C content. 13C content (calculated from total C content X atom-% ^{13}C) measured for all 8 HF replicates of individual samples for which ^{13}C NMR spectra were acquired (left column), and for individual samples for which ^{13}C NMR spectra were acquired (right column). Error bars represent 1 SD. Significant differences by Tukey's HSD (p-value = 0.05) between timepoints are indicated by letters. Atom-% ^{13}C, total C, and total ^{13}C values for the HF samples for which ^{13}C NMR spectra were acquired (right column) label each bar. Colors represent timepoints and correspond to spectra represented in Supplemental Figure 2.

Characteristic	Field Site: HREC

Location	39°00'14.6"N 123°05'09.1"W
Elevation (m)	244
MAT (°C)	14
MAP (cm)	94
Soil type	Typic Haploxeralf
Series name	Squawrock-Witherell Complex
Bulk density	1.457 g/cm3
Aggregate stability	39 +/- 7
CEC (meq/100g)	18.75
SOC (mg/g soil)	13.1 +/- 1.7
TN (mg/g soil)	1.3 +/- .1
C/N	9.7 +/- .4
Texture	48, 35, 17
Clays (30%)	Muscovite (17.8%) Chlorite (11.8%) Kaolinite (0.7%)
Non-clays (70%)	Quartz (47.3%) Plagioclase (22.4%)
pH (Spring)	5.9 +/- .1
pH (Fall)	7.3 +/- .1
Soil Moisture % (Spring)	14.3 +/- 2.6
Soil Moisture % (Fall)	1.9 +/- .3

Table 1. Site characteristics and soil physicochemical properties. Location and soil pedological information determined via NRCS Web Soil Survey. Elevation and climate characteristics described by HREC. Soil texture and CEC determined by UC Davis analytical lab. Mineralogy determined at LLNL. Aggregate stability defined as % water-stable aggregates, was measured on soil collected March 2018. DOC, SOC, TN, C/N was collected in Spring 2018; pH and soil moisture was sampled in Spring 2018 during the rainy season and fall 2018 during the dry season.

Time after 13C labeling	Ecosystem pool	Total C pool (g / m2)	Total 13C pool (mg 13c / m2)	% of plant-fixed 13CO2 remaining

0 days	**Total**	**7152 +/- 899**	**12887 +/- 3321**	**100%**
	Aboveground	146 +/- 39	7699 +/- 3066	60%
	Belowground (roots + soil)	7006 +/- 888	5187 +/- 1160	40%
4 weeks	**Total**	**7464 +/- 997**	**8188 +/- 2307**	**64%**
	Aboveground	158 +/- 60	4729 +/- 1969	37%
	Belowground (roots + soil)	7307 +/- 1007	3459 +/- 1588	27%
	FLF	795 +/- 186	489 +/- 217	(4%)
	OLF	1274 +/- 356	468 +/- 449	(3.6%)
	HF	4043 +/- 849	2130 +/- 740	(16.5%)
6 months	**Total (soil)**	**9058 +/- 874**	**8247 +/- 3058**	**64%**
	FLF	1003 +/- 230	3012 +/- 1588	(23.4%)
	OLF	1236 +/- 217	627 +/- 318	(5%)
	HF	4691 +/- 922	2883 +/- 808	(22.4%)
1 year	**Total (soil)**	**8267 +/- 1319**	**4797 +/- 3778**	**37%**
	FLF	936 +/- 202	1128 +/- 725	(8.8%)
	OLF	1428 +/- 407	467 +/- 429	(3.6%)
	HF	3982 +/- 570	2246 +/- 1080	17.4%)
2 years	**Total (soil)**	**7072 +/- 999**	**2910 +/- 2072**	**23%**
	FLF	534 +/- 155	390 +/- 338	(3%)
	OLF	1090 +/- 496	285 +/- 322	(2%)
	HF	3468 +/- 583	1480 +/- 1010	(11.5%)

Table 2: Distribution of ^{13}C label within ecosystem pools. We defined 100% remaining plant-fixed $^{13}CO_2$ as that present in the system (aboveground + belowground pools) immediately after the $^{13}CO_2$ labeling period ("0 days" timepoint). The aboveground pool consists of aboveground plant biomass, and the belowground pool consists of root biomass + bulk soil. For the "6 months", "1 year" and "2 year" timepoints, ^{13}C-labeled roots had senesced and so were not measured separately from the bulk soil was done for the "0 days" and "4 weeks" timepoints. The

bulk soil was further separated into three sub-pools via soil density fractionation, yielding the free-light fraction (FLF), occluded-light fraction (OLF), and heavy fraction (HF). Average ^{13}C recovery based on FLF + OLF + HF was about 72% that of the bulk soil, which is within the range for C recovery in density fractionated soil generally cited in the literature (Crow et al., 2007; Cusack et al., 2018).

Sampling time	Density Fraction	Total C (mg/g)	Total N (mg/g)	C/N Ratio	δ 13C	Total 13c (ug/g)	Dry mass (g)
Spring 2018	FLF	1.6 +/- .5 b	.08 +/- .03 b	19.9 +/- 3.0 c	30.1 +/- 26.6	0.9 +/- 0.4 b	.1 +/- .03
	OLF	2.1 +/- .6 b	.1 +/- .03 b	17.5 +/- 1.1 b	-0.8 +/- 18.7	0.8 +/- 0.8 b	.1 +/- .03
	HF	7.1 +/- 1.6 a	.9 +/- .1 a	8.2 +/- .6 a	21.9 +/- 14.4	3.7 +/- 1.3 a	19.5 +/- .2
Fall 2018	FLF	1.9 +/- 6 b	.09 +/- .03 b	20.7 +/- 2.8 c	238.0 +/- 74.4	5.3 +/- 2.8 a	.2 +/- .04
	OLF	2.3 +/- .6 b	.1 +/- .04 b	17.5 +/- 1.0 b	23.2 +/- 26.9	1.2 +/- 0.4 b	.1 +/- .03
	HF	7.8 +/- 1.6 a	.9 +/- .1 a	8.5 +/- .5 a	30.7 +/- 17.1	5.0 +/- 1.4 a	19.4 +/- .2
Spring 2019	FLF	1.6 +/- .4 b	.09 +/- .02 b	19.1 +/- 1.8 c	78.3 +/- 57.2	2.0 +/- 1.3 ab	.1 +/- .04
	OLF	2.4 +/- .6 b	.1 +/- .04 b	17.3 +/- .9 b	12.9 +/- 17.9	1.1 +/- 0.6 b	.1 +/- .04
	HF	7.1 +/- 1.6 a	.8 +/- .1 a	8.5 +/- .8 a	24.5 +/- 20.5	3.9 +/- 1.9 a	19.4 +/- .2
Spring 2020	FLF	0.9 +/- .2 c	.05 +/- .01 b	18.7 +/- 2.1 b	51.3 +/- 64.4	0.8 +/- 0.6 b	.1 +/- .03
	OLF	1.8 +/- .7 b	.1 +/- .04 b	17.8 +/- .8 b	0.4 +/- 16.6	0.6 +/- 0.6 b	.1 +/- .04
	HF	6.3 +/- 1.1 a	.8 +/- .1 a	8.0 +/- .6 a	15.8 +/- 19.3	2.9 +/- 1.6 a	19.6 +/- .2

Table 3: Characteristics of soil density fractions. Means shown +/- 1SD. Elemental characteristics are shown in units of quantity of element per gram of soil. $\delta^{13}C$ values represent absolute ^{13}C enrichment. Total ^{13}C values represent total ^{13}C added during the ^{13}C labeling period (calculated from atom-% excess ^{13}C). Dry mass (g) value represents quantity of starting soil sample (~20g) recovered in each density fraction.